INTERNATIONAL JOURNAL OF HYDROGEN ENERGY 47 (2022) 33781–33802

Available online at www.sciencedirect.com

ScienceDirect

journal homepage: www.elsevier.com/locate/he

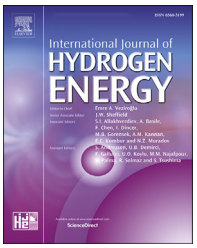

Toward underground hydrogen storage in porous media: Reservoir engineering insights

Esuru Rita Okoroafor[*], *Sarah D. Saltzer*, *Anthony R. Kovscek*

Stanford University, United States

HIGHLIGHTS

- Reservoir and operational parameters that enable large-scale hydrogen storage in depleted gas reservoirs are investigated.
- Reservoir simulation and sensitivity analyses provide insights into hydrogen dynamics in depleted gas reservoirs.
- The top factors impacting hydrogen withdrawal are reservoir depth, dip, current pressure, and flow capacity.
- Hydrogen recovery per cycle depends on reservoir structure, properties, and management practices.
- Novel screening and scoring criteria are developed to select potential porous media underground hydrogen storage sites.

ARTICLE INFO

Article history:
Received 28 March 2022
Received in revised form
11 June 2022
Accepted 28 July 2022
Available online 29 August 2022

Keywords:
Underground hydrogen storage
Geological formations
Numerical simulation
Sensitivity analyses
Depleted gas reservoirs
Site selection criteria

ABSTRACT

Subsurface hydrogen storage in depleted hydrocarbon reservoirs and saline formations is a potential option for storing hydrogen at large scales. These subsurface formations need to store sufficient hydrogen efficiently and securely, and the hydrogen must be withdrawn in adequate quantities on demand. In this study, we investigate the reservoir, geological, and operational controls that enable large-scale hydrogen storage and maximize hydrogen injection and withdrawal from depleted natural gas reservoirs. Hydrogen injection, storage, and withdrawal scenarios were computed using a reservoir simulator. Sensitivity analyses exposed the crucial parameters to achieve the goal of optimum storage and withdrawal of hydrogen. We determined that reservoirs with smaller pressures at the start of storage operations are suitable for hydrogen storage if wellhead pressure constraints permit. Steeply dipping reservoirs enable better hydrogen withdrawal if the reservoirs have good permeability (greater than 100 mD) and the injection/withdrawal well is placed updip within the reservoir. Permeable reservoirs and reservoirs with sufficient thickness increase hydrogen withdrawal rates. These findings and the results of the sensitivity analyses are used to propose site selection criteria for underground storage of hydrogen in depleted gas reservoirs.

© 2022 Hydrogen Energy Publications LLC. Published by Elsevier Ltd. All rights reserved.

* *Corresponding author.*
E-mail address: ritaok@stanford.edu (E.R. Okoroafor).

https://doi.org/10.1016/j.ijhydene.2022.07.239

0360-3199/© 2022 Hydrogen Energy Publications LLC. Published by Elsevier Ltd. All rights reserved.

Nomenclature

φ	Effective porosity, fraction
k	Absolute permeability, mD
p	Pressure, bar
T	Temperature, °C
UHS	Underground Hydrogen Storage
BHP	Bottom-hole pressure, bar
E	Compression energy, GJ
PI	Productivity Index, $Sm^3/d/bar^2$
Greek	
γ	Polytropic index for hydrogen

Introduction

Anthropogenic emissions of carbon dioxide and other greenhouse gases present one of the world's most pressing challenges. Decarbonization mechanisms such as energy-efficient buildings and vehicles, energy-conserving pathways, changes in land use, carbon capture and storage, and fuel switching are all being pursued aggressively. Fuel switching replaces high carbon-emitting fuels with clean, renewable fuels to decarbonize energy sectors such as electricity and heat for homes and commercial buildings, transportation, and industrial processes.

Renewable energy resources such as solar and wind provide emissions-free electricity. Renewable resources, however, are seasonal and have intermittent electricity generating capacity. Surplus electricity produced from these resources can be converted to hydrogen using electrolysis, where water is split into hydrogen and oxygen. The hydrogen may be stored and later converted back to electricity to power the grid or sent directly to homes for heat. Because hydrogen can be converted to electricity or heat, the hydrogen becomes an efficient energy carrier capable of transporting and storing energy with much less loss (<0.1%) than in a power network (8%), according to Ref. [1]. Hydrogen may also be derived from natural gas using steam methane reforming (SMR), autothermal reforming (ATR), or coal gasification. SMR and ATR release carbon dioxide but, when combined with carbon capture and storage technology, can lead to net-zero emissions, thus contributing to a carbon-neutral global economy.

Hydrogen can be stored in liquid or gaseous form. Well-known hydrogen storage technologies include compressed gas cylinders, liquid tanks, metal hydrides, and carbon structures [1,2]. For large-scale energy storage, hydrogen storage technologies may not suffice as large amounts of storage volume are needed. As an alternative, hydrogen can be stored underground in geological formations, including salt structures (caverns), saline aquifers, or depleted natural gas reservoirs.

In addition to having sufficient capacity, underground hydrogen storage in geological reservoirs reduces the risk of explosion. Salt caverns have successfully stored hydrogen with a high degree of purity, as they are completely airtight and pose a low risk of contamination to the gas through chemical reactions or consumption of the hydrogen by microbes when compared to other geological reservoirs [1,3]. Salt caverns, however, are geographically scarce and have limitations in capacities, with the largest single salt cavern having a hydrogen storage capacity of 906,000 Sm^3 [4]. Porous media such as aquifers and depleted natural gas reservoirs are not constrained by geography. The abundance of these geological reservoirs, including their significant storage capacities, make them attractive for large-scale hydrogen storage. While there is experience with gas storage in porous media, there are no cases of pure hydrogen storage in aquifers or depleted gas fields reported in the literature.

Challenges with underground hydrogen storage in porous geological formations

[5] conducted an extensive investigation of the technical and economic feasibility of storing hydrogen gas in underground reservoirs. They studied a depleted field, an aquifer, a salt cavern, and an excavated rock cavern. They used analytical equations to represent the volume of hydrogen stored at any given pressure and temperature, the gas flowrate, and the water movement with hydrogen withdrawal. Their study demonstrated that there were no technical limitations for storing hydrogen underground in porous media. Despite the findings by Ref. [5]; the experience with underground hydrogen storage in porous geological formations is limited by practical applications to the storage of town gas, i.e., gas mixtures with 25–60% hydrogen, and smaller amounts of CH_4 (10–33%), CO and CO_2 (12–20%) and <30% N_2. Several reviews discuss the challenges with hydrogen storage in the subsurface [4,6–11]. These reviews identified loss of hydrogen due to microbial growth in the reservoir, geochemical reactions within the reservoir, and mixture of hydrogen with the residual or cushion gas as challenges [6,7,10,11]. Moreover, reviewers noted that uncontrolled lateral spreading of hydrogen, hydrogen leakage through faults or the caprock, cyclical stress fluctuations, and clay-swelling induced stresses are essential considerations in choosing storage sites [7,9]. Laboratory experiments can address the knowledge gaps related to the aforementioned challenges. Numerical simulation studies, however, provide an opportunity to model the complex, interwoven physics relevant to the underground hydrogen storage in porous geological formations across several scales. Hence, the thrust of this paper is the role of numerical modeling and simulations in allowing for a broader range of research and sensitivity analyses that are essential to supplement laboratory experiments.

Previous insights from numerical simulation studies

Several numerical simulation studies expanded knowledge of underground hydrogen storage in porous media. [12,13]; and [14] studied hydrogen storage behavior in a subsurface porous media site using ECLIPSE 300, a numerical reservoir simulator. Nitrogen was the cushion gas. The gases were modeled as first-contact miscible fluids using the Peng Robinson Equation of State. The studies showed that the hydrogen withdrawal rate increased with the number of storage cycles while the amount of water extracted declined with each storage cycle [15]. Used the ECLIPSE 100 Solvent Model and conducted

numerical simulations of seasonal hydrogen storage in the Norne hydrocarbon field, offshore Norway. In their model, they treated hydrogen as a solvent that is not immediately miscible with the reservoir oil and gas. Three different storage schemes were examined by injecting pure hydrogen into the gas, oil, and water zones. They implemented four annual withdrawal-injection cycles followed by one prolonged withdrawal period. Their study showed that the thin gas zone was a preferred target with a roundtrip hydrogen recovery factor of 87%. Their study also showed that placing the injector well lower in the dipping structure results in lower storage efficiency.

The choice of the cushion gas may impact the recovery and purity of hydrogen recovered from underground hydrogen storage [16]. Used a 2D numerical simulation model, combined with scaling theory, to investigate the impact of CO_2 as a cushion gas for H_2 flow in a heterogeneous subsurface aquifer system. They studied a 10 m $\times$ 80 m system and a rescaled system of 30 m $\times$ 240 m. They determined that hydrogen infiltrates the cushion gas in the proximity of the injectors preventing an efficient piston-like displacement of the CO_2. They also deduced that hydrogen recovery performance was poorer in viscous-dominated flow regimes while the best recovery performance occurred in gravity-dominated regimes [17]. Used the numerical simulation model of a real oilfield hosting heavy crude oil in a heterogeneous carbonate reservoir rock to investigate the role of methane, nitrogen, and carbon dioxide as cushion gases in underground hydrogen storage in a depleted oil reservoir. Their study revealed that methane performs better as the cushion gas compared to nitrogen and carbon dioxide [18]. Examined the effect of cushion gas on underground hydrogen storage in a partially depleted gas condensate reservoir. They used a numerical simulation model representing the depleted carbonate gas condensate field. The cushion gases were methane, nitrogen, and carbon dioxide. The highest and the lowest hydrogen recovery and purity were obtained by injecting nitrogen and carbon dioxide as cushion gas, respectively.

[19] investigated the effects of gas rising, lateral spreading, and hydrodynamics for underground hydrogen storage using the open-source code DuMu^x. The gas-phase density was calculated using the ideal gas law, while the gas-phase viscosity was calculated by the Wilke method that correlates the viscosity dependent on composition and temperature. Their study showed that for small injection rates, gravitational forces were dominant and allowed for uniform displacement of water. In contrast, viscous forces become dominant at greater injection rates, and the water displacement becomes unstable with lateral gas fingers propagating below the caprock toward the left and right boundaries of the reservoir [20]. Investigated the effects of gas mixing, seasonal injection and production cycles, and hydrodynamics of underground hydrogen storage using DuMu^x and COMSOL multiphysics. Similar to Ref. [19]; the gas-phase density was calculated using the ideal gas law, while the gas-phase viscosity was calculated with the Wilke method. Their study showed that gravity override and viscous fingering in the aquifer play a minor role in impacting the efficient displacement of the native fluid if the reservoir is gas saturated. Their results showed an average hydrogen concentration of the extracted gas of 82 mol% in the first production cycle and increased to 85.2 mol% during the last production cycle.

[21] compared the respective capacities and deliverabilities of hydrogen to established natural gas in a seasonal storage facility in the UK. In addition, they used PHREEQC, a geochemical modeling tool, to investigate the chemical stability and potential losses due to the interaction of the different fluids present in the reservoir. Their study showed that hydrogen loss due to dissolution and diffusion were less than 0.1% while, in the worst-case scenario, no more than 3.7% of the hydrogen was lost due to conversion to methane and biomass over the lifetime of the storage scheme [22]. Showed that lateral fingers were more pronounced in underground hydrogen storage than in natural gas storage scenarios.

[23] assessed strategies for seasonal underground hydrogen storage in a saline aquifer using COMSOL multiphysics. Gas-phase density was evaluated using the Peng–Robinson equation of state, while the gas viscosity and water hydrodynamic properties were calculated with the built-in Comsol state equations. Their study showed that a maximum 78% hydrogen roundtrip recovery could be achieved and that steeply-dipping reservoirs stored hydrogen without needing cushion gas but were prone to water cresting. Hydrogen recovery was best achieved using extraction wells completed just below the caprock and wells that did not extend over the full reservoir thickness [24]. Used PetraSimTOUGH2 compositional numerical simulator to evaluate the viability of seasonal hydrogen storage in a deep aquifer. Their results showed that the maximum saturation with hydrogen takes place around the injection well, and hydrogen spreads along the top of the reservoir just below the caprock [25]. Examined the effect of caprock availability and hydrogen injection rate on the hydrogen recovery from a heterogeneous porous reservoir. They concluded that high injection rate increases H_2 leakage in the absence of a caprock, and lower injection rates and caprock availability increase the amount of recovered hydrogen.

[26] conducted a sensitivity analysis to understand the effect of storage parameters on hydrogen storage capacity. Their study showed that the reservoir pressure, the working gas capacity fraction, and the irreducible water saturation had the most significant potential to change the storage capacity. The greater the reservoir pressure, the larger the working gas capacity fraction, and the lower the irreducible water saturation, the more hydrogen that could be stored. Their study does not determine how the reservoir pressure, the working gas capacity fraction, and the irreducible water saturation affect the amount of hydrogen recovered, which is the ultimate goal of underground hydrogen storage.

The aforementioned numerical studies, combined with laboratory experiments and field implementation, guide site selection criteria to optimize underground hydrogen storage. However, they are not exhaustive on possible geological and reservoir controls that impact underground hydrogen storage.

State-of-the-art in site selection criteria for underground hydrogen storage in porous media

[24] suggested further studies on underground hydrogen storage in deep aquifers should be directed at determining the optimum depth of the gas store [27]. Determined the optimal

depth to maximize the mass of hydrogen in underground storage to be 1100 m, while [28] suggest that suitable offshore hydrogen storage reservoirs should be at depths over 1500 m to ensure that hydrogen densities of 10 kg/m^3 are achieved. Because hydrogen density increases with increasing pressure and reducing temperature, the influence of pressure is more significant than temperature.

The reservoir depth is not the only parameter determining if a site is suitable for underground hydrogen storage [29]. Proposed site selection criteria for pure hydrogen storage in porous geological media. They suggested a minimum depth of 500 m, a maximum depth of 2500 m, a dipping reservoir over a flat reservoir, effective porosity of more than 10% for sandstones and greater than 5% primary porosity for carbonates, and a minimum of 10 mD permeability for carbonates while a minimum of 50 mD for sandstone reservoirs. However, their study does not explain how they arrived at most of the criteria. Some additional criteria were qualitative rather than quantitative [30]. Used Fuzzy-Delphi methodology to prioritize the criteria and sub-criteria that seemed to be most relevant for the underground hydrogen storage site selection process. They extracted eighteen criteria from the literature consisting of technical, economic, health, safety and environment, and social points of view. From their results, the most important sub-criteria identified include legal restrictions, reservoir permeability and porosity, and regional risks. The ranking they deduced is more applicable as a weighting factor in the site selection process because it does not provide a rating for the parameters that are relevant for underground storage site selection.

The aim and scope of this study

While the existing studies provide some insights into the behavior of hydrogen stored in porous media and provide some guidance on underground hydrogen site selection criteria, detailed geological and reservoir controls that impact underground hydrogen storage remain poorly understood.

Our study evaluates the significance of geological parameters for underground hydrogen storage in depleted gas reservoirs. We investigate the reservoir, geological, and operational controls to enable large-scale hydrogen storage and maximize hydrogen injection and withdrawal using a numerical reservoir simulation approach. The novelty of this study is the insight we provide on the impact of different geologic and reservoir controls on underground hydrogen storage, as well as a systematic, reservoir-engineering approach to developing screening criteria for potential future underground hydrogen storage sites. Furthermore, we provide a methodology to rank the geological and reservoir properties of potential underground hydrogen storage sites. This solution does not currently exist in the literature.

The organization of the paper is as follows. First, we describe the hydrogen injection and withdrawal scenario examined. This is followed by the numerical simulation modeling parameters we use. We then describe the key metrics used to analyze the data. Subsequently, we analyze the results and discuss the implications of the results. Finally, based on the findings from the results, we propose site selection criteria.

Methods

Scenario description

Using the work of [13] as a guide, we modified the injection and withdrawal cycles to recreate the scenario for the present study. There are six storage cycles with a withdrawal period of one week per cycle. The first storage cycle lasts for 210 days at a target rate of 150,000 Sm^3/d before the first withdrawal cycle. The storage is replenished for 50 days at a target rate of 150,000 Sm^3/d after a ten-day shut-in subsequent to each withdrawal period. The next storage cycle follows after an additional shut-in period of 10 days, resulting in one withdrawal phase every two months. Fig. 1 shows the scenario.

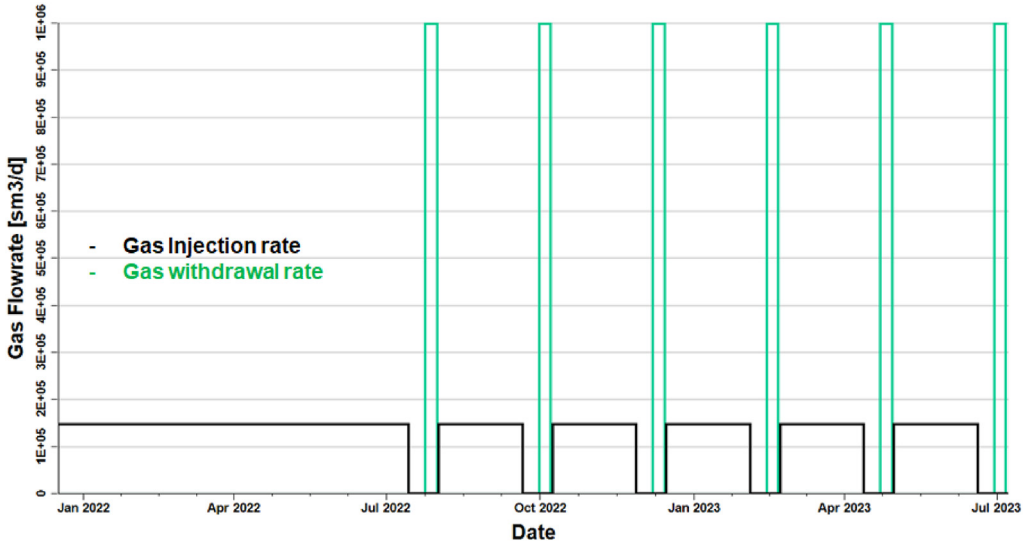

Fig. 1 – Injection and withdrawal rates over the duration of the study.

Table 1 – Parameters used in the model and other calculations related to this study.

Symbol	Description	Value	Units
φ	Porosity of the reservoir	0.2	–
k_H	Horizontal reservoir permeability	4.9×10^{-13}	m^2
k_V	Vertical reservoir permeability	4.9×10^{-14}	m^2
T_r	Average reservoir temperature	43	°C
k_{rgc}	Critical gas saturation	0.05	–
k_{rwc}	Critical water saturation	0.20	–
p_r	Average reservoir pressure	80	bar
GIP	Gas in place (methane)	4.69×10^9	Sm^3
c_r	Rock compressibility	1.01×10^{-4}	bar^{-1}
p_{ref}	Reference pressure for fluid density	1.013	bar
ρ_{H2}	Hydrogen density at reservoir conditions	5.98	kg/m^3
μ_{H2}	Hydrogen dynamic viscosity at reservoir conditions	8.20×10^{-6}	Pa·s
ρ_{CH4}	Methane density at reservoir conditions	55.28	kg/m^3
μ_{CH4}	Methane dynamic viscosity at reservoir conditions	1.31×10^{-5}	Pa·s
T_{ref}	Reference temperature for fluid density	15.56	°C
ρ_f	Water density	999.7	kg/m^3
c_w	Water compressibility at reservoir conditions	2.0×10^{-4}	bar^{-1}
B_w	Water formation volume factor at reservoir conditions	2.0×10^{-4}	m^3/Sm^3
μ_w	Water dynamic viscosity at reservoir conditions	6.18×10^{-4}	Pa·s
P_{in}	Inlet pressure for compressor at point of injection	2	bar
P_{out}	Outlet pressure for compressor at the point of distribution	50	bar
γ	Polytropic index for hydrogen	0.29	

Reservoir numerical model

We model a hypothetical reservoir to understand the reservoir and geological controls that enable large-scale hydrogen storage and maximize hydrogen injection and withdrawal. Hydrogen is injected into a depleted gas reservoir, with the remaining natural gas (methane) used as the cushion gas. ECLIPSE E300, a multiphase-multicomponent simulation code, was used to run the reservoir simulation [12]. And [13,14] demonstrated that this simulation code could suffice for modeling hydrogen storage and transport in porous media. The numerical simulation model is a 3000 m by 3000 m reservoir with a spatial discretization of 30 m × 30 m in the lateral direction. The reservoir thickness is 100 m with a cell thickness of 5 m in the z-direction. The cell sizes were smaller than that used for the model in Refs. [13–15]. We performed a grid refinement study to ascertain that the cell sizes were sufficient to capture the behavior of hydrogen while minimizing computational time. The details of the grid refinement study are presented in Appendix A on "Grid Refinement Study". The reservoir is flat with the top of the reservoir at a depth of 1000 m. The reservoir for the base case simulation is considered homogenous in porosity and permeability. The base case parameters are provided in Table 1. Fig. 2 shows the simulation domain.

We determined the rock compressibility using Newman's correlation for consolidated sandstone reservoirs [31] given by

$$c_f = \frac{97.3 \times 10^{-6}}{[1 + 55.9\varphi]^{1.429}} \quad (1)$$

In the base case, a single well injects 150,000 Sm^3/day of hydrogen. The target withdrawal rate is set to 1,000,000 Sm^3/day. The well is placed at the center of the reservoir and is perforated over the top 30 m of the reservoir. The injector well serves as the withdrawal well.

We determined the density of methane (CH_4) and hydrogen (H_2) using a generalized formulation of the Peng–Robinson equation of state [32]. We obtained binary interaction coefficients (BIC) from Ref. [33]. As part of the ECLIPSE E300 software, gas-phase viscosities were computed using the Lorentz-Bray-Clark (LBC) correlation. With the parameters used in this study, the densities (Table 1) obtained for reservoir conditions are within 1.9% and 2.2% of the values given in Ref. [34] for H_2 and CH_4, respectively. Viscosity values for H_2 and CH_4 deviated by up to 12.2% and 1.5% respectively from those given in Ref. [34]. However, these values are still within the uncertainty range given in Ref. [34]; that are 15% and 2% for H_2 and CH_4, respectively.

The hydrogen relative permeability used in the study was determined from the work by Ref. [35] and was input as tables into the simulation. We did not model hydrogen-methane relative permeability separately. We assumed the hydrogen relative permeability defines the behavior of the gases in the reservoir as both gases will be mixed in the reservoir. However, we expect the difference in flow behavior between the gases to be driven by the difference in mobility for the gases because hydrogen should be lower viscosity. The simulation included gas dissolution in connate water. The solubility of hydrogen in water at 43 °C was taken from Ref. [36]; while the solubility of methane in water at 43 °C was taken from Ref. [37]. The actual values used are presented in Appendix B.

The reservoir pressure was considered depleted to 80 bar at a datum depth of 1050 m, about 20 bar below the hydrostatic pressure for that depth. The caprock was assumed to be tight against the stored H_2 and CH_4 and was thus represented in the simulation as a no-flow boundary. Diffusion within the gas phase was neglected, and no geomechanical effects were considered during the simulation. No degradation of hydrogen via reaction was incorporated.

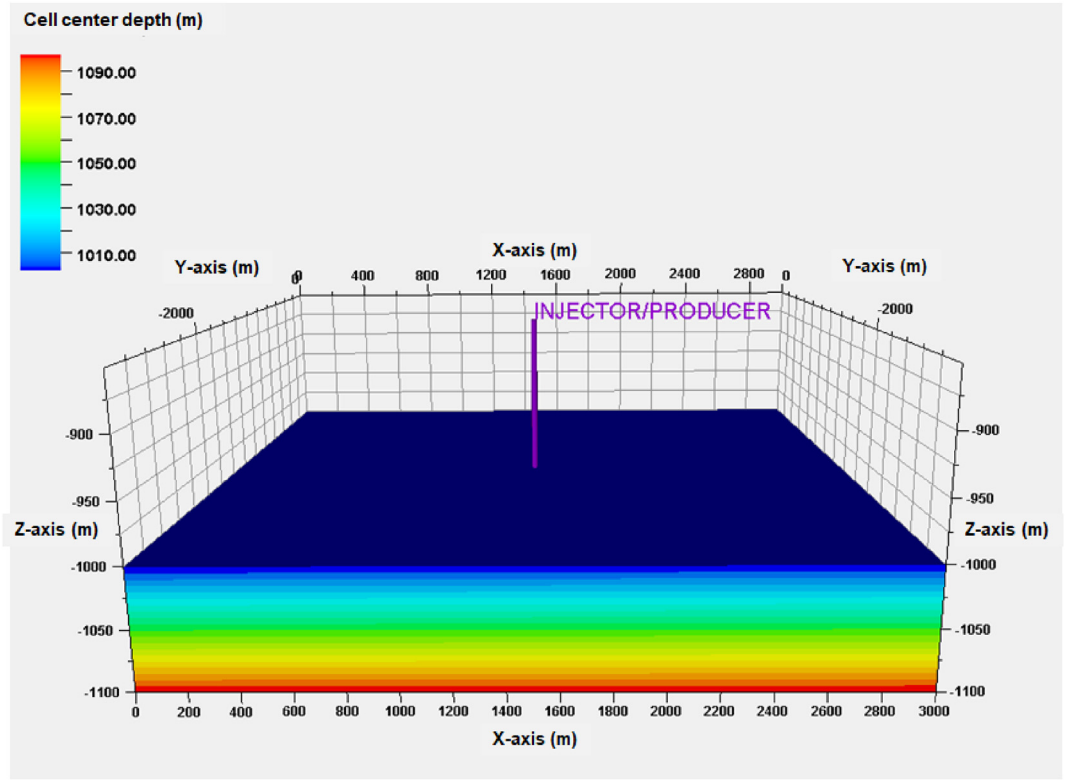

Fig. 2 – Numerical simulation domain showing the depth of the reservoir. The figure is not drawn to scale.

Because this model was not designed for a specific field or reservoir, we set the maximum and minimum allowable BHPs to 120 bars and 30 bars at the reservoir top depth. The specified upper BHP limit corresponds to typical overbalance margins used during drilling, ranging from 20 bar to 35 bar [38]. In case of a violation of the BHP limits, the simulator automatically adapts the well flow rate until the pressure is within the specified range. The minimum allowable BHP was set to allow for a 10-bar pressure drop between the bottom hole and the wellhead, assuming a tubing head pressure (THP) of 20 bar. The wellbore had a nominal diameter of 0.3 m. Skin effects on the well flow rates were neglected.

We initialized the model by enumeration through specifying an average gas saturation of 0.3. Once the model equilibrates, gravity segregation occurs with high gas saturation at the top of the reservoir. This results in 30% of the reservoir thickness occupied by the reservoir gas and the remaining 70% occupied by water.

Sensitivity analysis

The first stage of the sensitivity analysis was to identify parameters that impact the productivity index of hydrogen withdrawal. The productivity index is a common subsurface engineering metric to gauge a well's productivity or to compare the productivity of different wells, as it normalizes the flowrate using the energy (pressure) required to produce the fluid. The productivity index is defined as the flow rate per unit pressure drop. The expression for the gas flow rate is determined from the theoretically derived inflow performance relationship (IPR) equation for gas production at reservoir pressures below 137 bar [39] and is given by

$$q_g = \frac{C_1 kh\left(p_R^2 - p_{wf}^2\right)}{T\mu_g Z\left[\ln\left(r_e/r_w\right) - 0.75 + s\right]} \quad (2)$$

where

q_g is the gas flow rate, p_R is the reservoir pressure, p_{wf} is the wellbore bottomhole flowing pressure, T is temperature, Z is the gas compressibility factor, μ_g is the gas viscosity; r_e is the drainage radius, r_w is the wellbore radius, and s is the skin factor.

Table 2 – Parameters and corresponding values for the first-stage sensitivity analysis.

Parameter	0.5 × Base value	Base value	1.5 × Base value	Units
Reservoir Area	4500000	9000000	13500000	m^2
Porosity	10	20	30	%
Permeability	250	500	750	mD
Top of Reservoir	500	1000	1500	m
Formation Thickness	50	100	150	m
Current Reservoir Pressure[a]	60	80	100	bar
Geothermal Gradient	14	28	42	C/km
Formation dip[a]	−2	0	2	°

[a] The pressure and formation dip were not 0.5 and 1.5 of the base values.

We define the average productivity index (J) of the hydrogen withdrawn as

$$J = \frac{Q_g / t}{\left(p_R^2 - p_{wf}^2\right)} \tag{3}$$

where Q_g is the cumulative hydrogen withdrawn by the third (3rd) cycle, and t is the number of days of hydrogen withdrawal. We chose the 3rd cycle because that was when we began to observe notable differences between hydrogen recovered among different scenarios.

Table 2 shows the parameters evaluated, including their base values, as well as values used in the sensitivity analysis. When evaluating permeability, the k_v/k_h ratio was kept constant at 0.1. When evaluating the top depth of the reservoir, a 20% pressure depletion was imposed on the expected hydrostatic pressure expected at the reservoir depth. Because the perforation length was set to 30 m in the base case, the perforation interval was set to 30% of the reservoir thickness for cases examining the sensitivity of thickness. The solubility and the binary interaction coefficients were modified to correspond to the selected reservoir temperature for temperature sensitivity. We performed a multivariate polynomial regression fit on the [36] dataset to determine an equation for hydrogen solubility as expressed in Eq. (4) as

$$s = 0.2852p - 0.0149T - 0.0126p^2 - 0.0102pT + 0.0262T^2 + 0.3324 \tag{4}$$

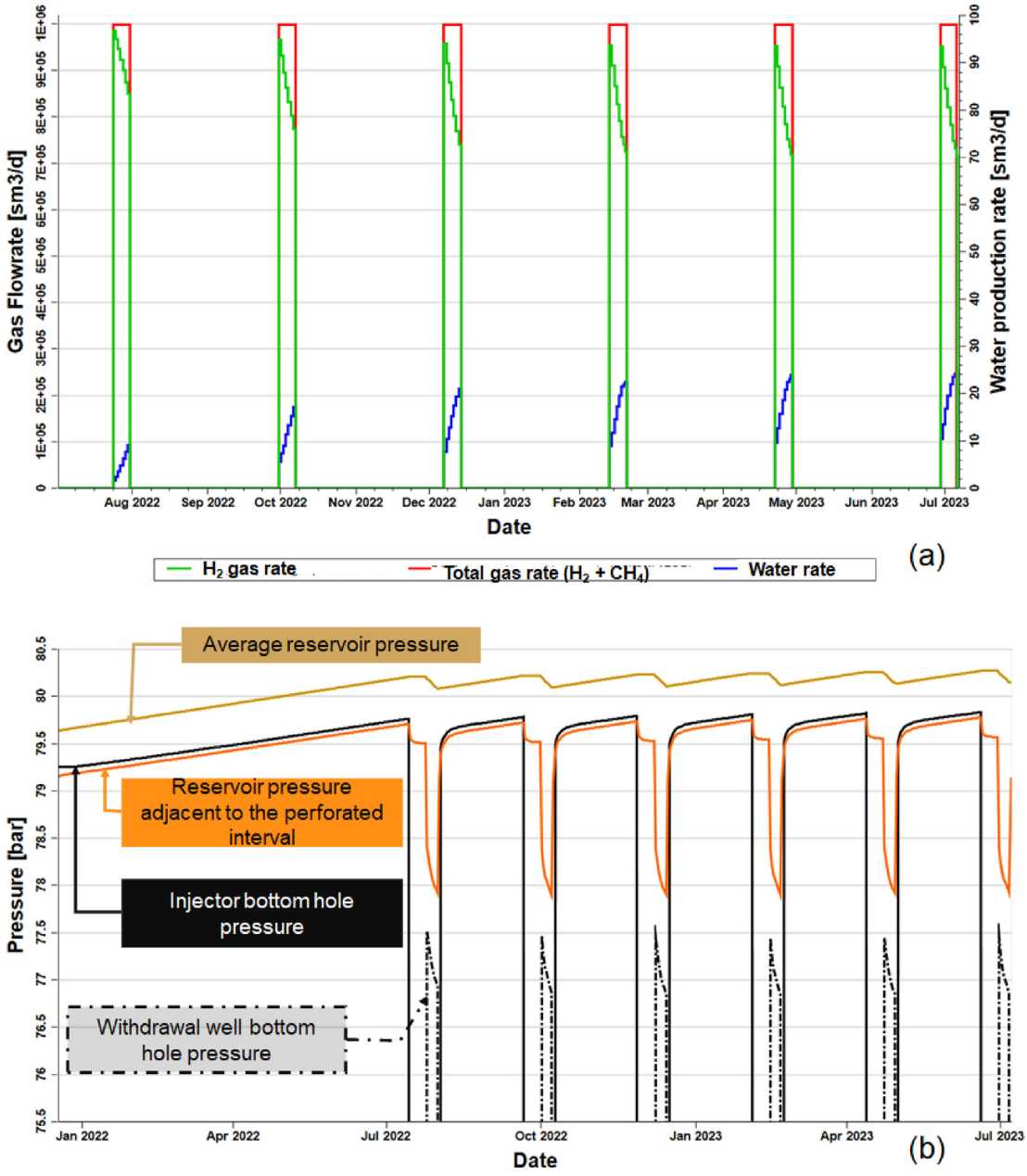

Fig. 3 – Rates and pressures for the base case. 3(a) shows the gas and liquid withdrawal rates. 3(b) shows the average reservoir pressures and the bottom hole pressures during injection and withdrawal.

Certain parameters were taken for further study in the second stage of the sensitivity analysis, including the porosity, reservoir thickness, absolute permeability, formation dip, and k_v/k_h ratio.

Energy for compression

In addition to investigating the factors required to improve hydrogen extraction from a depleted reservoir, it was necessary to understand the energy required to compress the hydrogen for storage and later extraction. The energy, *E*, for compression in GJ is modified for unit compatibility from the work by Ref. [40] and is given by

$$E = \frac{0.00989}{\gamma} P_{in} Q_{in} \left[\left(\frac{P_{out}}{P_{in}} \right)^{\gamma} - 1 \right] t \quad (5)$$

where γ is the polytropic index (0.29 for hydrogen), *P* is pressure (bars), Q is flowrate (m^3/d), *t* is in days, and the subscripts "*in*" and "*out*" refer to the low and high pressure sides of the compressor.

Hydrogen purity

The purity of hydrogen, in percentage, is calculated as the cumulative volume of hydrogen withdrawn at the end of a cycle (or total number of cycles) divided by the cumulative volume of gas withdrawn at the end of the cycle (or total number of cycles).

$$H_{2\ purity} = \frac{vol\ of\ H_2\ withdrawn\ (sm^3)}{vol\ of\ gas\ withdrawn\ (sm^3)} \times 100 \quad (6)$$

Results and discussion

Base case results

Fig. 3(a) shows the amount of hydrogen, methane and water withdrawn with each cycle for the base case, while Fig. 3(b) shows the bottomhole pressure and average field pressure during the injection and withdrawal cycle. From Fig. 3(a), the hydrogen withdrawal rate reduces with each cycle until the 6th cycle where it is similar to the rate in the fifth cycle. The reservoir gas, methane, is produced during the withdrawal of hydrogen and increases in rate with each cycle. By the 6th cycle, however, it begins to reduce. Water production occurs from the beginning of the cycle and increases with each subsequent cycle, indicating that the withdrawal rate is greater than the critical rate to prevent water cresting for this well and reservoir configuration. From Fig. 3(b), we see that the injector bottom hole pressure does not exceed the 120 bar maximum limit, and is marginally above the reservoir pressure adjacent to the perforated interval.

Fig. 4 shows the mole fraction of hydrogen and fluid contacts at the beginning and end of the first and third injection-withdrawal cycles. The Gas-Water Contact (GWC) represents the depth above which there is predominantly gas and below which there is predominantly water. The black vertical lines in the figures represent the perforated interval. Fig. 4(a) shows the mole fraction of hydrogen after injecting hydrogen for the first cycle while Fig. 4(b) shows the hydrogen mole fraction after withdrawing gas. Fig. 4(c) shows the same information but after hydrogen has been injected for the third cycle while Fig. 4(d) shows the hydrogen mole fraction after withdrawing gas for the third cycle. Fig. 4(e) shows the hydrogen mole fraction after the third cycle but with the Z-axis presented to scale relative to the X- and Y- axes.

From Fig. 4(b) and (d), we see that some hydrogen remains in the reservoir after each withdrawal, with more hydrogen left at the top of the reservoir.

Sensitivity analysis for parameters that affect hydrogen productivity from depleted gas reservoirs

Fig. 5 shows the tornado plot of the parameters that affect the productivity index (PI) of the withdrawn hydrogen after being

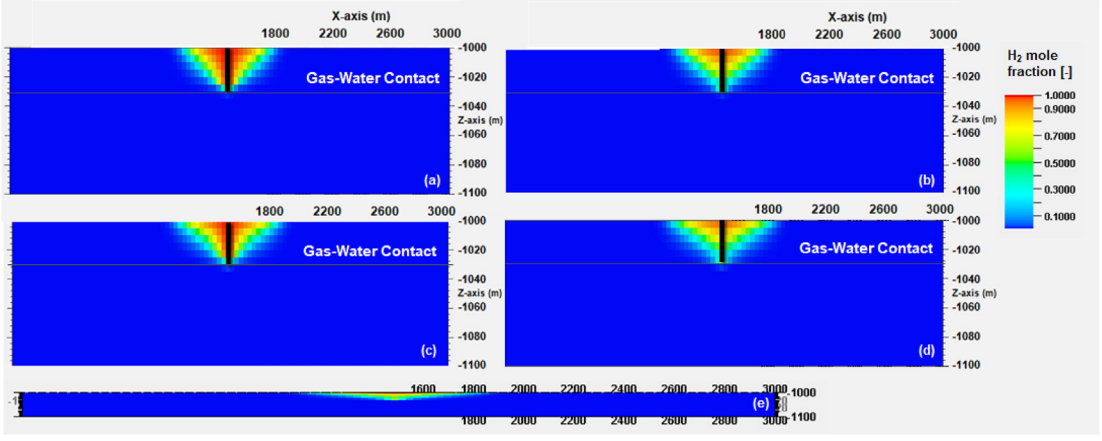

Fig. 4 – Mole fraction of hydrogen at the beginning and end of the first and third injection-withdrawal cycles. Vertical well position denoted in black. Fig. 4(a) shows the hydrogen mole fraction after hydrogen is injected for the first cycle. Fig. 4(b) shows the hydrogen mole fraction after hydrogen is withdrawn for the first cycle. Fig. 4(c) shows the hydrogen mole fraction after hydrogen is injected for the third cycle. Fig. 4(d) shows the hydrogen mole fraction after hydrogen is withdrawn for the third cycle. Fig. 4(e) shows the hydrogen mole fraction after the third cycle but with the Z-axis presented to scale relative to the X- and Y- axes.

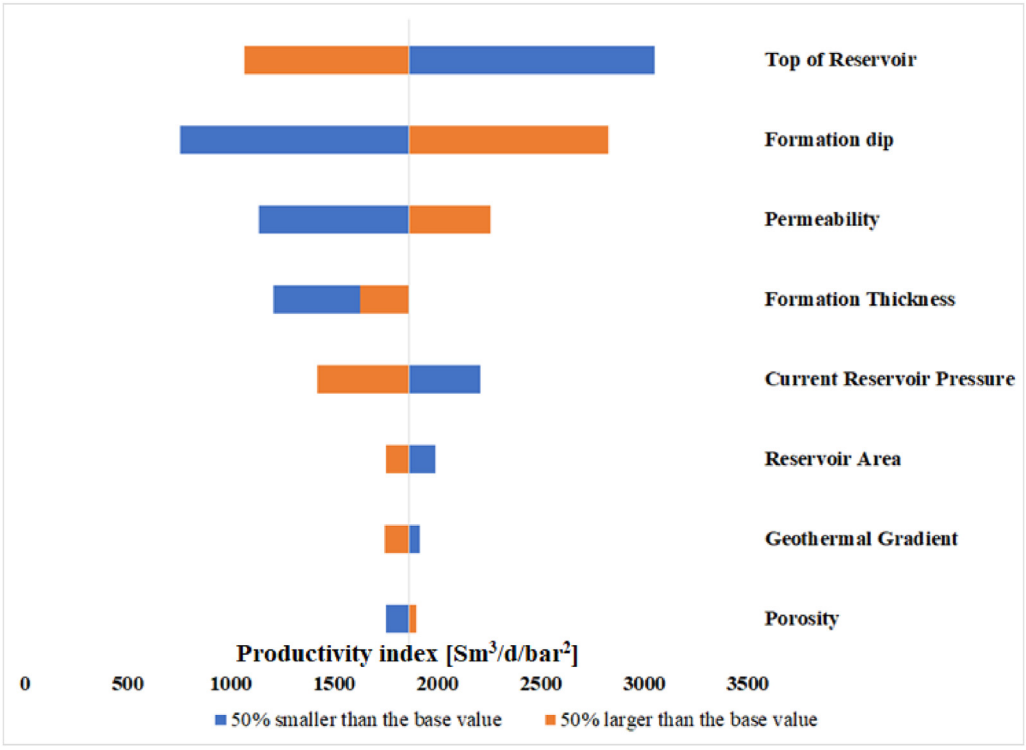

Fig. 5 – Tornado plot of parameters impacting the reservoir and geological controls of underground hydrogen storage in porous media.

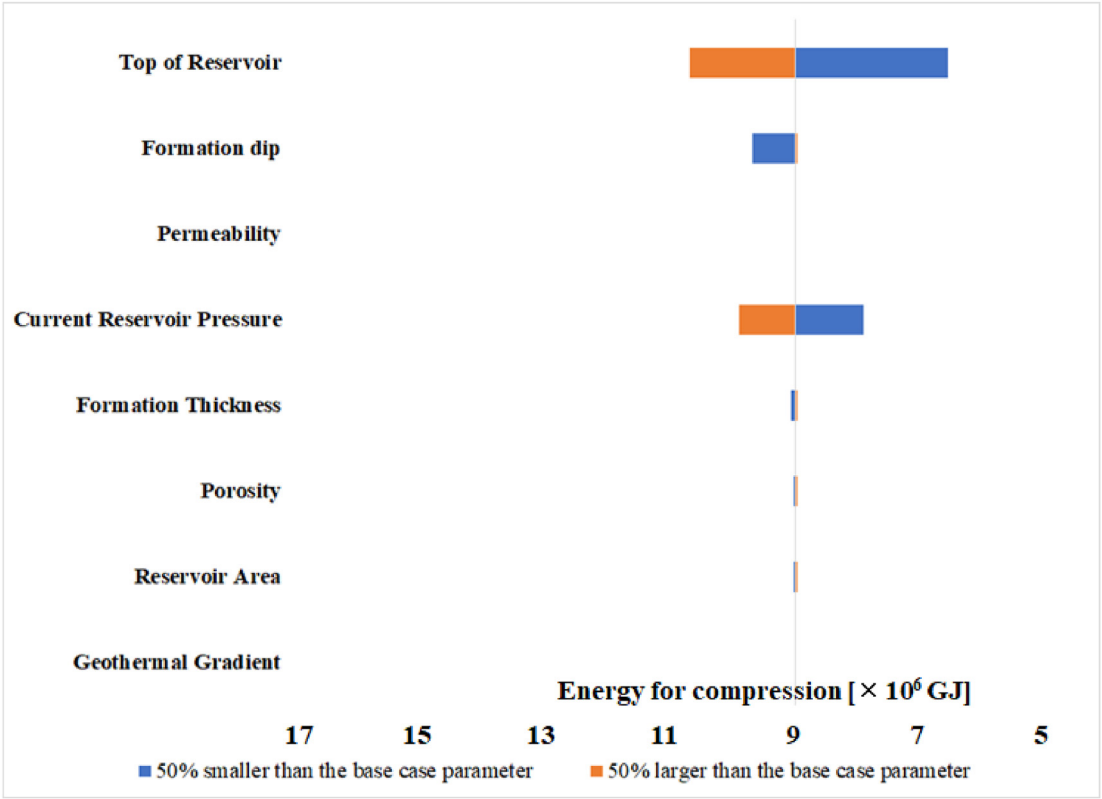

Fig. 6 – Compression energy required for the different scenarios. Values increase from right to left to demonstrate that larger compression energy is undesirable.

stored in a depleted gas reservoir. Bars to the right indicate that the selected value of the parameter results in increased hydrogen PI over the base case. In contrast, bars to the left indicate that the selected value of the parameter results in decreased hydrogen PI over the base case.

In Fig. 5 we see that having a shallow reservoir, having a dipping reservoir, having greater permeability than the base case permeability, and having small reservoir pressures are the top four factors that result in an increased PI of hydrogen. Small reservoir pressure and a shallow reservoir are interdependent parameters for a reservoir at hydrostatic conditions. However, this may not be the case for depleted reservoirs, as a deeper reservoir may have reduced reservoir pressure due to production. Hence, for depleted reservoirs, we will not focus on the depth but on the reservoir pressure, as the pressure can take any value at any depth for a depleted reservoir.

Placing the injector/withdrawal well downdip in a reservoir of 2° dip appears to impact negatively the PI of hydrogen much more than placing the wells updip. Though a formation thickness smaller than the base case thickness results in reduced PI, a 50% increase in the formation thickness also results in reduced PI, though not as much as when the formation thickness is reduced by 50%. This suggests that, for the scenario under study, there is an optimal formation thickness to maximize hydrogen withdrawal. Hydrogen recovery can also be improved in a reservoir with a smaller area than the base case, smaller geothermal gradient, and porosity larger than the base case. However, these parameters do not have as much impact as the top depth of the reservoir, formation dip, permeability, reservoir pressure, and formation thickness. The porosity was the parameter with the most minor influence on hydrogen PI.

Energy required for compression

The energy required for compression for each parameter investigated is presented in Fig. 6. Values increase from right to left to demonstrate that larger compression energy is undesirable. The compression energy is the energy required to compress the hydrogen from its source to the reservoir condition. For this study, we used 2 bars as the compressor inlet pressure at the point of injection and we used the injection well's maximum BHP as the compressor outlet pressure.

Fig. 6 demonstrates that the parameters that cause an increase in compression energy requirements over the base case are high reservoir pressure and placing the well downdip of the reservoir structure. The elevated reservoir pressure could be due to the existing reservoir pressure or the pressure that comes with having a deep reservoir. Hence, the top of reservoir is a factor that impacts the compression energy. For the case of placing the well downdip of the reservoir during injection, there is significant pressure buildup when displacing water compared to the base case or to having the well placed updip of the structure. Because the location of the wells had to be moved relative to the base case, a separate scenario was run to determine the effects of placing the well close to the boundary, and these effects were considered when estimating the PI from the wells placed updip and downdip of the reservoir. Fig. 7 shows the hydrogen mole fraction for different dip scenarios, while Fig. 8 shows the corresponding BHPs during injection and withdrawal.

The impact of reservoir depth and pressure on productivity index and compression energy

[5] identified compression cost as a significant contributor to the overall cost of underground hydrogen storage projects.

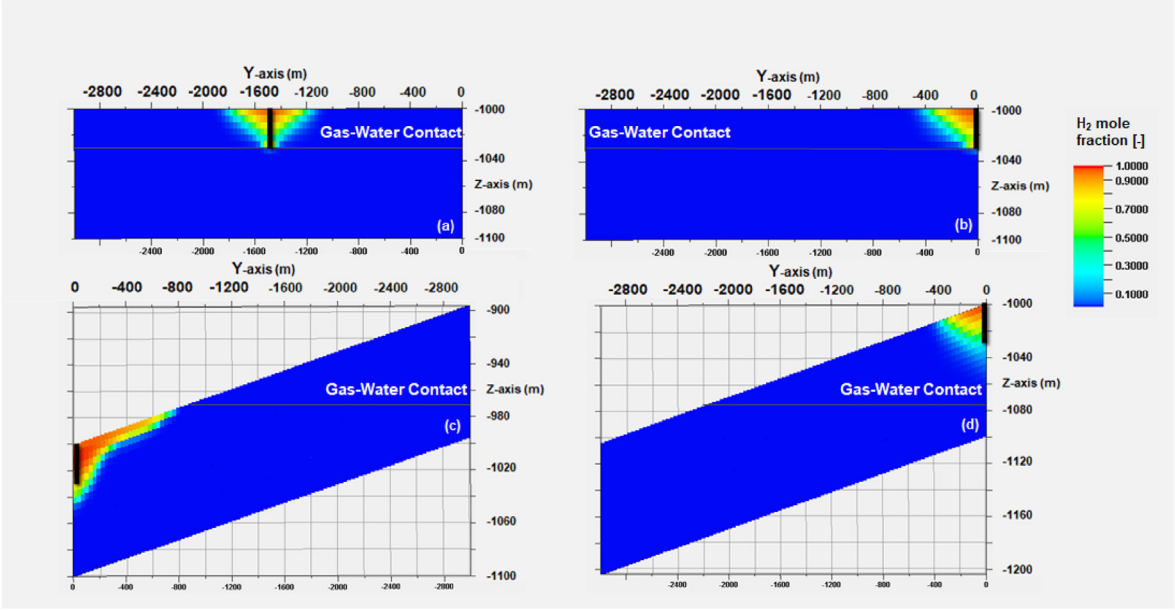

Fig. 7 – Dip scenarios for productivity index and compression energy sensitivity analysis: (a) is the base case, (b) is the case with the well placed at a boundary, (c) is for the scenario where the well is placed downdip of the structure, (d) is for the scenario with the well placed updip of the structure.

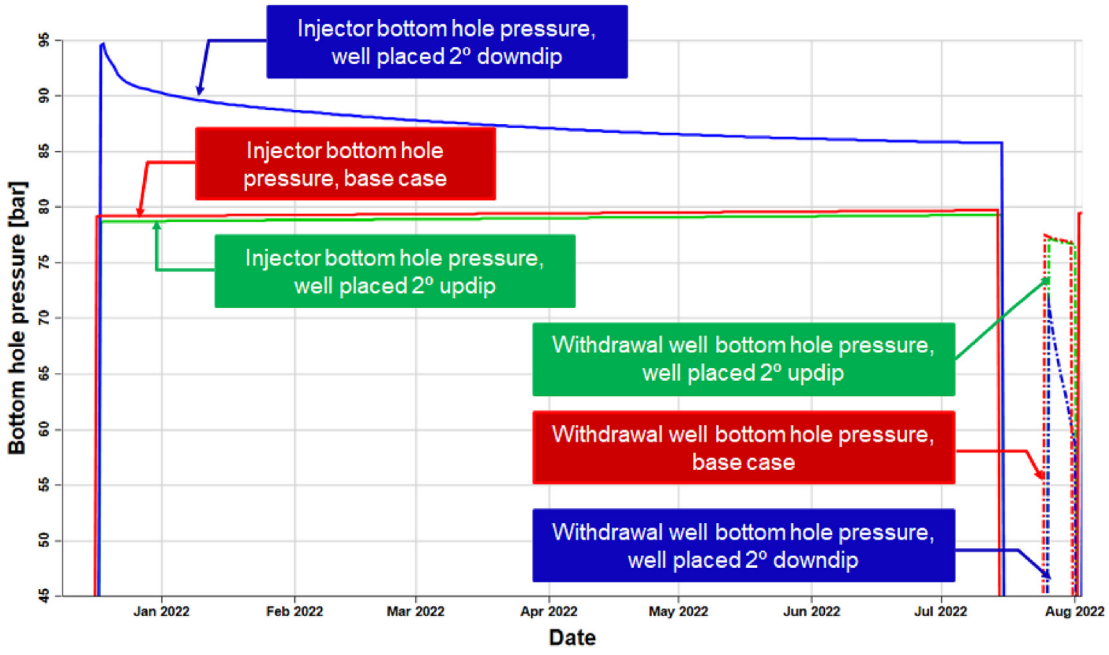

Fig. 8 – Bottom hole pressures for the injectors and withdrawal wells used in the sensitivity analysis on formation dip.

Therefore, in addition to maximizing the PI of hydrogen, it is also imperative to optimize the compression cost, a parameter that is inferred from the compression energy required. In Fig. 9, we present the productivity index and compression energy estimated for different depths. The compression energy increases from top to bottom of the chart. We highlight that for a depleted gas field, the depth is not the factor that drives the productivity or compression energy required, as the pressure in depleted fields varies based on the volume of fluid produced and production practices. Thus, pressure is the factor that drives the productivity and compression energy required for depleted fields. However, for saline reservoirs and

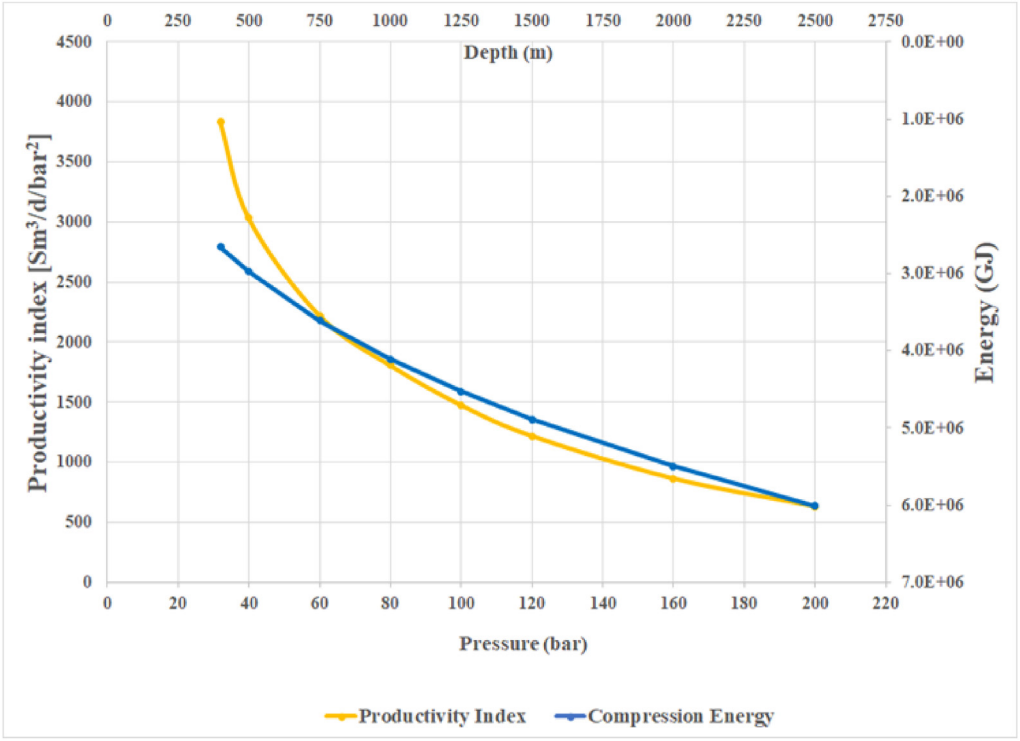

Fig. 9 – Productivity index (left) and compression energy (right) for the stored hydrogen at different reservoir pressures. The pressures are based on a 20% depletion of the hydrostatic pressure at the reservoir depth.

non-depleted oil and gas reservoirs, the static reservoir pressures have not been disturbed by fluid withdrawal, and, thus, the depth correlates with the reservoir pressure in a normal pressure regime. In such a scenario, the depth can be used as a site selection criterion.

From Fig. 9, the PI decreases with increased pressure and depth. In addition, the compression energy increases with increased pressure and depth. Due to this increased compression energy and reduced PI with depth, we propose 3000 m as a maximum depth for storing hydrogen. We did not compute the PIs for reservoir pressures below 32 bar as the simulations were based on a withdrawal well bottom hole pressure limit of 30 bar. Thus, we suggest that the tubing head pressure, wellhead pressure, or surface facilities' pressure be used as the constraint to determine the minimum reservoir pressure for geological storage of hydrogen in a depleted gas field. We modeled the pressure losses during injection and withdrawal of hydrogen. The details are available in Appendix C, "Wellbore Flow Modeling". From the wellbore pressure losses computed, we suggest that if the reservoir pressure is known, the wellhead pressure can be estimated by subtracting 1 bar/100 m from the reservoir pressure to determine if the reservoir pressure meets the surface pressure constraints.

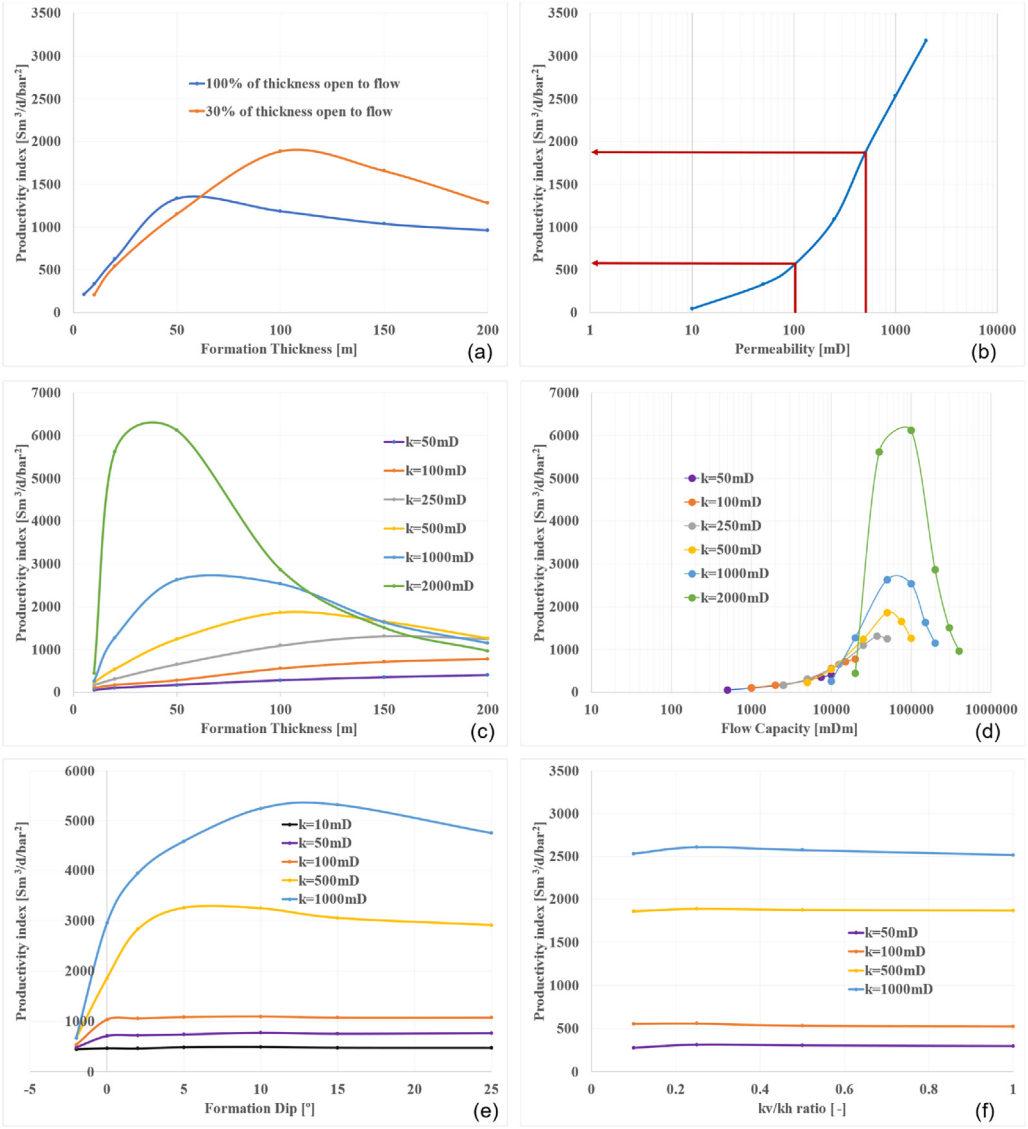

Fig. 10 – Hydrogen productivity indices for different sensitivity analyses scenarios. 10(a) shows the PI versus formation thickness for a scenario where the reservoir is completely open to flow (blue) and another scenario where 30% of the reservoir is open to flow (orange). 10(b) shows hydrogen PI versus absolute reservoir permeability. The red lines show how the PI at 100 mD and 500 mD. The PI at 100 mD is three times less than the PI at 500 mD. 10(c) shows hydrogen PI versus reservoir thickness for different absolute permeabilities. 10(d) shows hydrogen PI versus flow capacities for various formation permeabilities. 10(e) shows hydrogen PI as a function of dip angle for different permeabilities. 10(f) shows hydrogen PI as a function of permeability anisotropy ratio for different permeabilities. (For interpretation of the references to color/colour in this figure legend, the reader is referred to the Web version of this article.)

Further sensitivity analyses

Sensitivity analysis on reservoir thickness

The tornado plot in Fig. 5 showed that increasing or reducing the reservoir thickness would result in a smaller PI compared to the base case PI. To investigate this further, we considered reservoir thicknesses of 10 m, 20 m, and 200 m, in addition to the base case thickness of 100 m and the 50 m and 150 m that we initially evaluated and presented in Fig. 5. We consider two scenarios. In the first scenario, 30% of the reservoir was open to flow for all of the reservoir thicknesses. In the second scenario, the entire reservoir thickness was open to flow. We also added a 5 m reservoir thickness to the second scenario. Fig. 10(a) shows the PIs over different depths for the two scenarios. For the case where 30% of the reservoir was open to flow, the optimal depth was around 110 m. However, for the case where the entire reservoir thickness was open to flow, the optimal depth was approximately 50 m. Beyond 60 m, the PI was smaller than in the case with 30% of the reservoir open to flow due to the production of other competing fluids including methane and water.

Sensitivity analysis on absolute permeability

The Tornado plot in Fig. 5 shows that the PI of hydrogen increased by 20% with a 50% increase in permeability while reducing the permeability by 50% resulted in a 40% reduction in the hydrogen PI. Additional sensitivity analysis was performed to understand how the hydrogen productivity would be impacted by different absolute permeabilities. This sensitivity analysis is shown in Fig. 10(b).

The overall trend indicates that increased absolute reservoir permeabilities are favorable for hydrogen recovery. Below 100 mD, the productivity index drops below 500 $Sm^3/d/bar^2$, more than three times the productivity of the base case with a permeability of 500 mD. For screening of reservoirs, we suggest that sandstone reservoirs with permeabilities below 50 mD be excluded. For ranking, reservoirs with larger permeabilities will be rated better than those with smaller permeabilities.

Sensitivity analysis on flow capacity

The flow capacity, denoted by kh, is the product of the reservoir's absolute permeability and thickness. The trend in

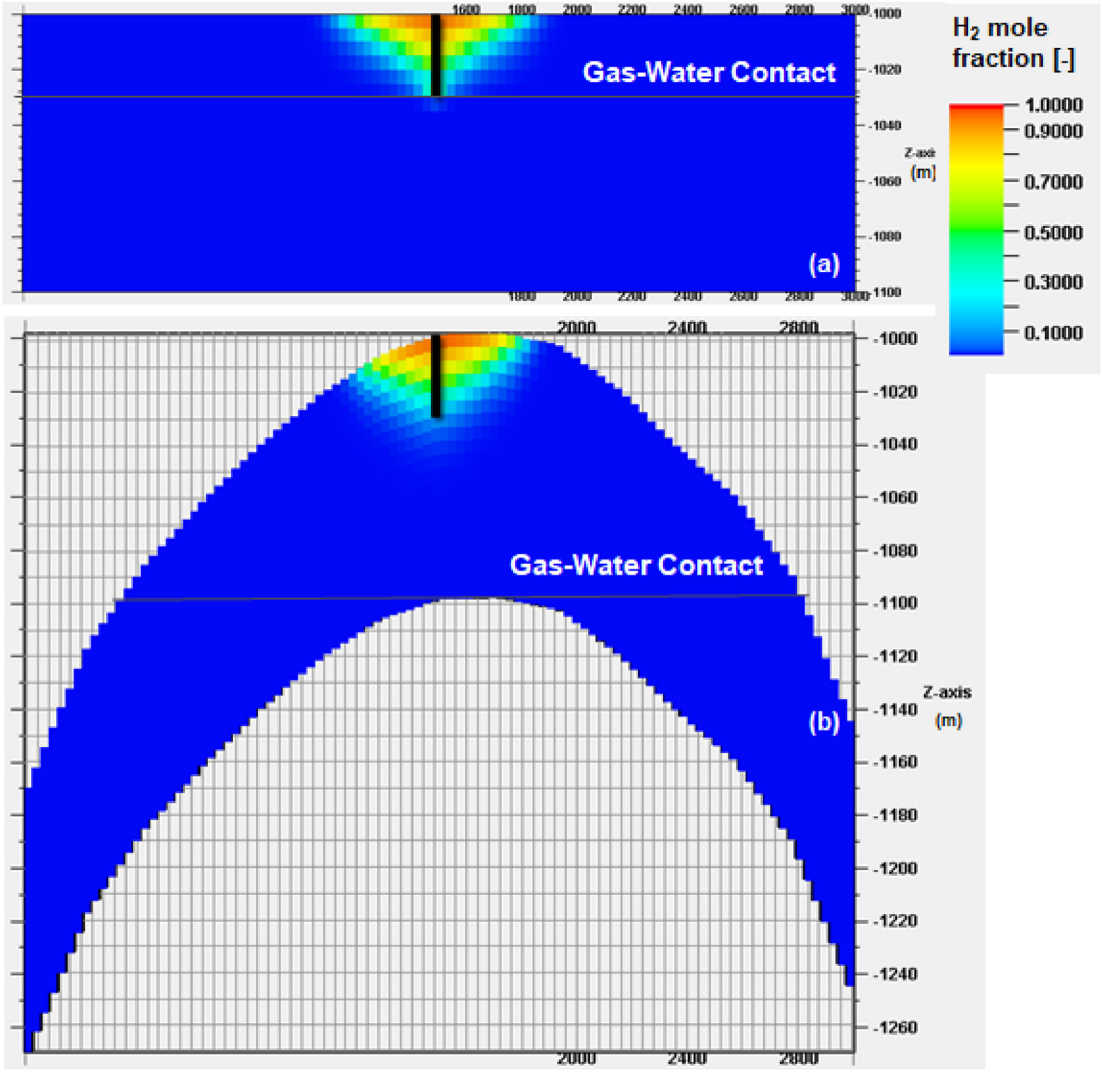

Fig. 11 – Cumulative hydrogen produced as a function of dip angle for different permeabilities.

Table 3 – Different scenarios for investigating the impact of heterogeneity on hydrogen productivity index.

	Layer 1 (mD)	Layer 2 (mD)	Layer 3 (mD)	Layer 4 (mD)	Layer 5 (mD)	Cumulative hydrogen withdrawn ($\times 10^6$ Sm^3)	BHP (bar)	PI ($Sm^3/d/bar^2$)	Permeability contrast (Ratio of permeability in the top layer to permeability in the layer that follows)
Base Case (Homogenous)	500	500	500	500	500	18.4	77.0	1863	1
High-Low-High-Low-High (HLHLH)	500	100	500	100	500	19.1	76.6	1657	5
Low-High-Low-High-Low (LHLHL)	100	500	100	500	100	19.5	73.0	841	0.2
Very low-High-Very low-High-Very low (VLHLHL)	50	500	50	500	50	19.2	70.3	593	0.1

Fig. 10(a) suggests that there is an optimal depth to maximize hydrogen productivity. We examined the hydrogen PI over different reservoir thicknesses and different reservoir permeabilities, as shown in Fig. 10(c). We deduce from Fig. 10(c) that there are optimal depths for different permeabilities. For instance, for a 2000 mD reservoir, the maximum PI is at 40 m, while for a 500 mD reservoir, the maximum PI is at 110 m. This indicates that the permeability or the thickness alone is insufficient to determine if a reservoir will be productive for hydrogen recovery, but that the flow capacity is a better indicator of hydrogen productivity.

In Fig. 10(d), we present the productivity indices from Fig. 10(c) as a function of flow capacity. The result shows there are ranges of flow capacities where productivity indices are small, another range where productivity indices are large, and another range of flow capacities where the productivity indices are somewhere in between. These ranges are useful for developing rating criteria for underground hydrogen storage site selection.

The impact of reservoir dip on hydrogen productivity

The sensitivity analysis presented in Fig. 5 shows that having a dipping reservoir and placing the injector/withdrawal well updip is favorable for hydrogen productivity and recovery. To understand to what extent the reservoir dip would be favorable for hydrogen productivity, we computed the productivity index for different reservoir dips and different reservoir permeabilities, as shown in Fig. 10(e). From Fig. 10(e), reservoirs with permeabilities below 100 mD do not benefit significantly from increased reservoir dips. However, the most permeable reservoirs, such as 500 mD and 1000 mD, have increased hydrogen PI with an increase in dip. The benefit of having steeply dipping reservoirs, especially for high permeability reservoirs, corroborates the study by Ref. [23]; where the steeply dipping structure of their reservoir model enabled retention of high quantities of hydrogen.

Sensitivity analysis on permeability anisotropy ratio (k_v/k_h ratio)

Throughout the sensitivity analyses, we used a k_v/k_h ratio of 0.1. We then performed a sensitivity analysis on different permeability anisotropy ratios for different absolute permeabilities, as shown in Fig. 10(f). Overall, the permeability anisotropy ratio was not a very sensitive parameter. For k_v/k_h ratios less than 0.5, there was some increase in the hydrogen PI. Above 0.5, the impact on the hydrogen PI was minimal. Thus, a reservoir with a small k_v/k_h ratio is preferred.

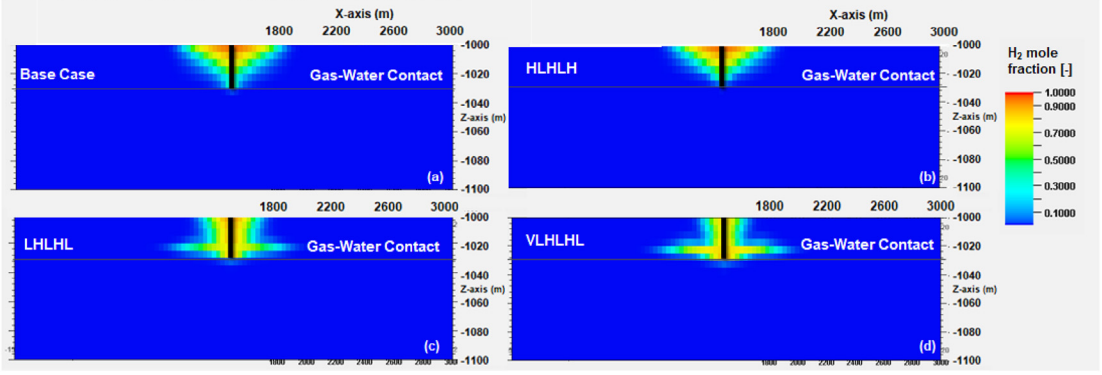

Fig. 12 – Mole fraction of hydrogen for the different scenarios on layer heterogeneity after the third injection and withdrawal cycle: (a) is the base case, (b) is the High-Low-High-Low-High (HLHLH) case, (c) is the Low-High-Low-High-Low (LHLHL), and (d) is the Very low-High-Very low-High-Very low (VLHLHL) case.

Table 4 – Different well architectures and their impact on the hydrogen productivity index.

	Cumulative gas withdrawn (× 10^6 Sm^3)	BHP (bar)	PI ($Sm^3/d/bar^2$)
Well Architecture			
1 Well: Injector/Withdrawal well (30 m perforated)	18.4	77.0	1863.3
1 Well: Horizontal Injector/Withdrawal well (30 m drain length)	18.9	76.8	1790.8
2 Wells: 1 Vertical Injector, 1 Horizontal Withdrawal well (30 m)	19.1	76.7	1761.6
1 Well: Injector/Withdrawal well (90 m perforated)	19.0	63.0	342.6
1 Well: Horizontal Injector/Withdrawal well (90 m drain length)	18.9	77.2	2043.6
1 Well: Horizontal Injector/Withdrawal well (300 m drain length)	18.5	78.4	3709.7
Perforation Length (m)			
30 (base case)	18.4	77.0	1863.3
5	18.9	71.8	703.0
10	18.8	75.0	1130.0
20	18.6	76.7	1708.5
35	18.6	75.5	1234.5

Table 5 – Estimated productivity indices and the hydrogen purity for different hydrogen withdrawal rates.

Gas rates (Sm^3/d)	Cumulative hydrogen withdrawn (× 10^6 Sm^3)	BHP (bar)	PI ($Sm^3/d/bar^2$)	Hydrogen purity %
500000	10.0	78.5	1878.7	95.4
750000	14.4	77.8	1926.4	91.6
1000000	18.4	77.0	1863.3	87.8
1500000	25.1	75.5	1748.8	79.7
2000000	30.4	73.7	1545.2	72.3

Impact of having a non-flat reservoir

In addition to examining the dip of the reservoir, we considered a scenario where the well was placed at the center of an anticlinal structure. At the end of the third injection and withdrawal cycle, the component mole fraction of hydrogen in the reservoir is as shown in Fig. 11. The PI for the base case (flat reservoir) was 1864 $Sm^3/d/bar^2$, while the PI for hydrogen from the anticlinal structure was 2313 $Sm^3/d/bar^2$. The pore volume was fixed for both scenarios. Hence, the improved PI from the anticlinal reservoir was because the gas-water contact was much deeper in the anticlinal case than in the base case to accommodate the same volume of gas. This resulted in reduced water cresting effects, less drawdown on the reservoir, and consequently a larger PI.

The impact of having heterogeneous layered reservoirs

To investigate the impact of heterogeneity on the PI of hydrogen from the depleted reservoir, we examined scenarios with different permeabilities in each layer. The 100 m reservoir thickness was divided into five layers of 20 m thickness. Table 3 shows the different scenarios, the associated

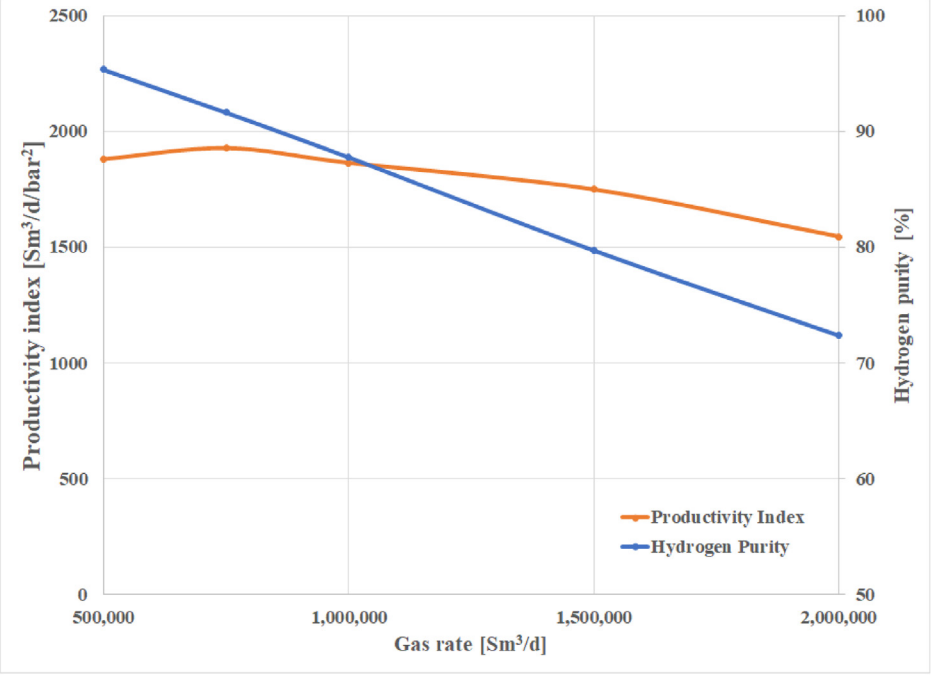

Fig. 13 – Impact of hydrogen withdrawal rates on the productivity index and hydrogen purity.

permeabilities in each layer, and the estimated PIs for each scenario. The layer count is from top to bottom of the reservoir.

From Table 3, we deduce that heterogeneity is not favorable for hydrogen extraction, as low permeability reservoirs within the perforated interval introduce increased drawdown pressures that lead to reduced PIs. The increased drawdown pressures can also result in cresting and more production of water. We define a permeability contrast as the ratio of the permeability in the top layer to the permeability in the layer that follows. A permeability contrast greater than one is better than a permeability contrast smaller than one. A more homogeneous reservoir is preferred for hydrogen storage.

Fig. 12 shows the hydrogen mole fraction for the different scenarios after the third injection and withdrawal cycle. Fig. 12(a) is the base case, Fig. 12(b) is the High-Low-High-Low-

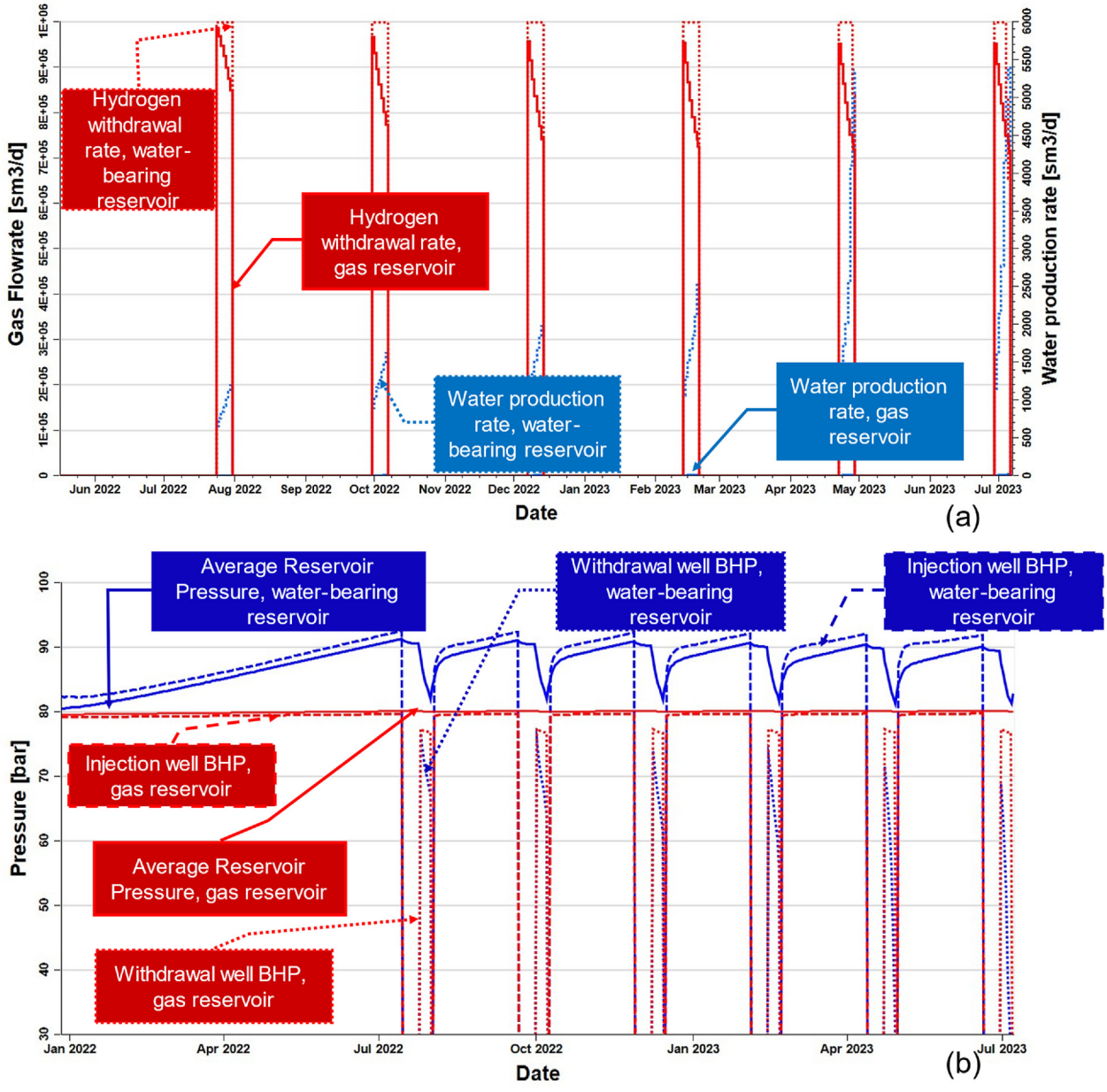

Fig. 14 – Comparison between pressure and withdrawal rates for a depleted gas reservoir and a water-bearing reservoir. 14(a) shows the hydrogen withdrawal and water production rates for the base case (depleted gas reservoir) and water-bearing reservoir. The solid lines represent the gas reservoir, while the dotted lines represent the water-bearing reservoir. The blue color indicates water production, while the red color represents the hydrogen withdrawal rate. 14(b) shows the bottom hole and average reservoir pressures for the base case (depleted gas reservoir) and the saline reservoir. The solid lines represent average reservoir pressures, the dash lines represent injection well bottom hole pressures, while the dotted lines represent withdrawal well bottom hole pressures. The blue color is for the water-bearing reservoir, while the red color is for the depleted gas reservoir. (For interpretation of the references to color/colour in this figure legend, the reader is referred to the Web version of this article.)

High (HLHLH) case, Fig. 12(c) is the Low-High-Low-High-Low (LHLHL), and Fig. 12(d) is the Very low-High-Very low-High-Very low (VLHLHL) case. In the low and very low permeability cases, Fig. 12(c) and (d), hydrogen in the permeable Layer 2 is hindered from upward flow by the smaller permeability in Layer 1, leading to hydrogen that would be difficult to recover.

Operational considerations

We investigated a few operational parameters to understand if they contribute to increasing the hydrogen productivity index. These parameters include the well architecture, the withdrawal rates, and the perforation depths.

Well Architecture

We explored the possibility of using horizontal wells for hydrogen extraction. Table 4 describes the different well architectures and their corresponding PIs.

In the base case, only 30 m of the reservoir thickness was perforated. Therefore, we considered a scenario where the horizontal well had only 30 m of drain length. The resulting PI of 1791 $Sm^3/d/bar^2$ was less than the PI of the base case, 1863 $Sm^3/d/bar^2$ determined for the vertical well. With a drain length of 90 m, we begin to see the benefit of having a horizontal well, with the well having a PI of 2043 $Sm^3/d/bar^2$. For a vertical well with 90 m of perforated interval, the PI is small due to water influx and high drawdown rates to drive the water that is produced. With 300 m of drain length, the PI increases to 3710 $Sm^3/d/bar^2$. Thus, horizontal wells are valuable if the drain lengths are sufficiently large to overcome pressure losses at the heel of the well.

Length of perforated zone

In the base case, the interval open to flow was just above the gas-water contact. The proximity to the gas-water contact may trigger water cresting and, hence, reduce hydrogen PI. We examined different perforation interval lengths (5 m, 10 m, and 20 m) to determine their impact on the PI of the well. The results are also presented in Table 4.

With smaller perforation interval lengths, the risk of water cresting is reduced; however, the smaller thickness available to flow also results in more pressure drawdown for the gas rate imposed during the simulation. This results in lower PIs. On the other hand, increasing the perforation interval to 35 m, allowing for 5 m in the water region, also results in a reduced PI due to water production. Hence, in this scenario, 30 m of perforation interval was optimal.

Withdrawal rates

We examined the impact of different gas withdrawal rates on the hydrogen PI. In addition, we estimated the hydrogen purity by the third injection and withdrawal cycle. Table 5 shows the different gas rates, the estimated PIs, and the hydrogen purity. In Fig. 13, the PIs and purity are plotted for each gas rate.

With increasing withdrawal rates, the drawdown increases, resulting in lower PIs. The hydrogen purity consistently reduced with increasing rates, starting from a purity of 95% for 500,000 Sm^3/d to 72% purity at 2,000,000 Sm^3/d. For the hypothetical reservoir being investigated, a withdrawal rate of 750,000 Sm^3/d appeared to be the optimal rate, resulting in the largest PI. This suggests a need for numerical simulation studies before implementing hydrogen storage projects to determine the optimal withdrawal rate.

The effect of injecting into a water-bearing reservoir

Thus far, we have considered a depleted gas reservoir with in situ methane as the cushion gas. We now consider a scenario where there is no in situ gas in the reservoir. This could either be a reservoir at residual gas saturation or a water-bearing reservoir (e.g. saline aquifers). We use the same injection and withdrawal cycle and rates as the depleted gas reservoir case. Fig. 14(a) shows the hydrogen and water withdrawal rates over the six injection/withdrawal cycles, while Fig. 14(b) shows the injection well bottom-hole pressures, withdrawal well bottom-hole pressures, and average reservoir pressure of both scenarios.

From Fig. 14(b), we observe that the pressure buildup in the water-bearing reservoir is much more than in the case of the depleted gas reservoir. Also with each cycle, the average reservoir pressure reduces, as can be observed from the fall-off periods. The consequence is that larger drawdowns are required to extract the required amount of hydrogen. In addition to having the hydrogen doubling as cushion gas, the

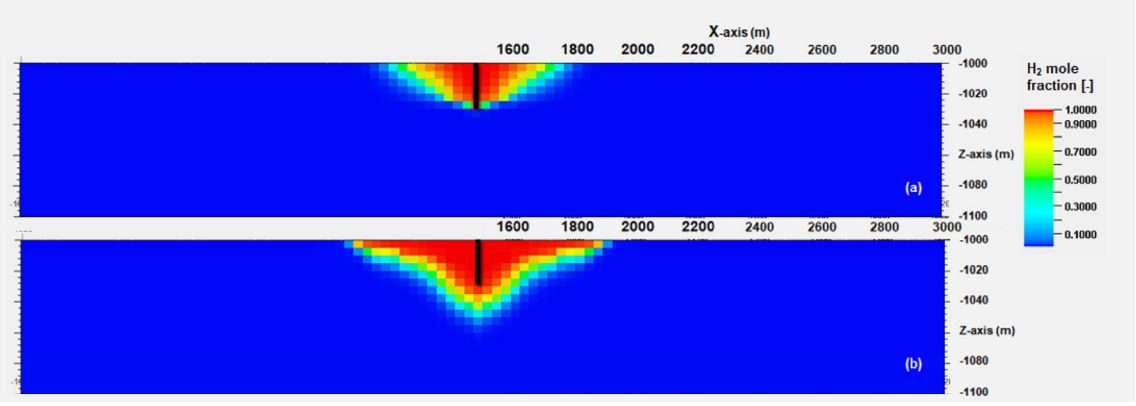

Fig. 15 – Extent of the hydrogen plume: 15(a) shows the spread of hydrogen within the depleted gas reservoir, while 15(b) shows the spread of hydrogen within the saline reservoir.

larger drawdown results in significant water production from the water-bearing reservoir (Fig. 14 (a)). The water production from the depleted gas reservoir, which was evident in Fig. 3 when the scale was from zero to 100 Sm^3/d, is negligible and can be barely seen in Fig. 14(a) that has a water production scale of zero to 6000 Sm^3/d.

Although the hydrogen production/withdrawal rates are larger for the water-bearing reservoir compared to the depleted reservoir, as seen in Fig. 14(a), the significant drawdowns lead to smaller PIs. At the third injection and withdrawal cycle, the estimated hydrogen PI is 461 $Sm^3/d/bar^2$, four times less than the PI when hydrogen is withdrawn from the depleted gas field.

Another parameter of interest is the distance from the well to the tip of the hydrogen plume. With hydrogen stored in the depleted gas reservoir having in situ methane as the cushion gas, the hydrogen plume tip extends to 320 m radius from the injection well. However, the hydrogen plume tip extends to 400 m radius from the injection well with the water-bearing reservoir. The extent of the plume is shown in Fig. 15.

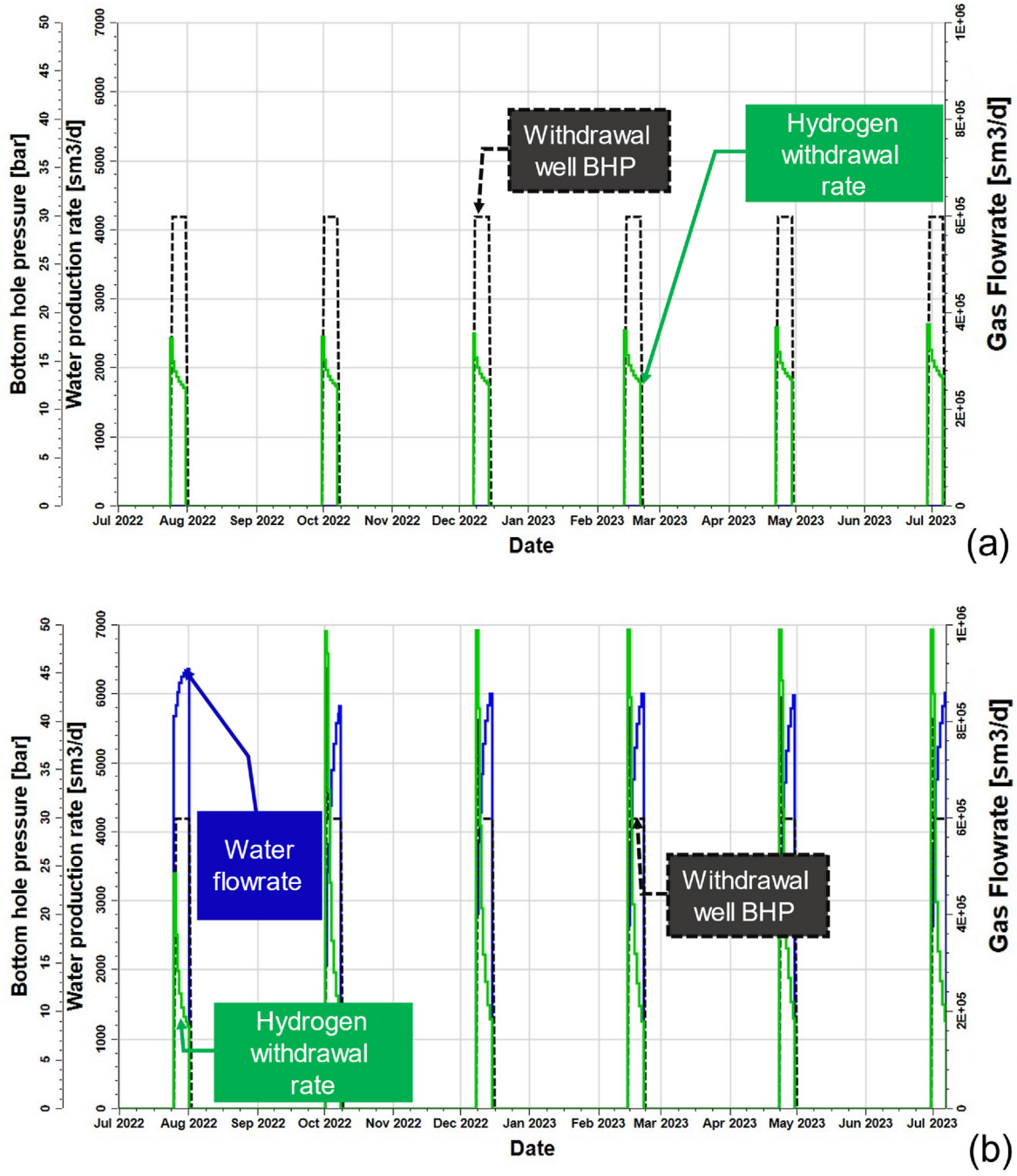

Fig. 16 – Hydrogen withdrawal rate, water production rates, and withdrawal well bottom hole pressures for (a) a reservoir with a permeability of 10 mD, and (b) when the reservoir is dipping at an angle of 10° with the well placed in the center of the reservoir.

Table 6 – Screening criteria for hydrogen storage optimization and risk minimization.

Category	Criteria	Disqualifying Threshold	Remarks
Hydrogen Storage and Withdrawal Optimization	Reservoir pressure	Wellhead Pressure Constraint > Pr-(0.01 bar/m) × reservoir top depth	There is a need to know if the current reservoir pressure can lift the hydrogen and other components that may be mixed with the gas for a depleted reservoir. The wellhead pressure constraint needs to be known.
	Maximum Depth of Top of Formation	>3000 m	At deeper depths, the productivity index of hydrogen reduces. Compression energy requirements typically increase with depth but this needs to be checked against the current reservoir pressure for a depleted field, as the more depleted a field, the less compression energy required.
	Permeability	<50 mD	
	Porosity	<10%	
	Net Reservoir Thickness	<10 m	
Risk and Hydrogen Loss Minimization	Top Seal Thickness	<20 m	[29]Bouteldja et al. (2021)
	Secondary Confining Units	No secondary confining units	This is a precautionary measure if hydrogen leaks from the reservoir in which it is stored. A secondary barrier is usually preferred.
	Active/Inactive Faulting	4 km wide "buffer zone" around all quaternary faults	[42]
	Resource in the reservoir	Oil or Gas Condensate	Reactions between hydrogen and liquid hydrocarbons are not well understood, and there may be possible reactions that could lead to hydrogen loss [7].
	Earthquake Record	10 km diameter for M > 5 (from 1769 – present), 5 km diameter for M < 5 (from 2015 – present)	[42]

Table 7 – Rating criteria for storage and injection optimization.

Criteria	1 (worst)	2	3	4	5 (best)	Remarks
Permeability Thickness	<1000 mDm	1000–10,000 mDm	10,000–40,000 mDm	>100,000 mDm	40,000–100,000 mDm	
Size (Storage Capacity); volume at stp	<1 MT (<12 km^3)	1–10 MT (12–120 km^3)	10–50 MT (120–600 km^3)	50–100 MT (600–1200 km^3)	>100 MT (1200 km^3)	
Permeability anisotropy	>0.8		0.5–0.8		0.1–0.5	
Porosity	<10%		10–30%		>30%	
Permeability Heterogeneity Contrast	<1		>1		1	The ratio of permeability in the top layer to permeability in the layer that follows
Reservoir Pressure	>220 bar	160–220 bar	80–160 bar	50–80 bar	<50 bar	Hydrogen embrittlement on tubulars is serious above 80 bar [5]; hence material selection is required for reservoirs above 80 bar
Reservoir dip		0–5 deg	>15 deg	10–15 deg	5–10 deg	This criterion assumes the well is placed updip of the structure
Reservoir Structure	Flat		Anticlinal/Moderately Dipping (<5 deg)		Steeply Dipping (>5 deg)	
Geothermal Gradient	Warm Basin (>40C/km)		Moderate (20–40 C/km)		Cold Basin (<20C/km)	

Comparison of findings from this study with other similar studies

Several studies investigating underground hydrogen storage in porous media (both depleted reservoirs and saline aquifers) have observed, for the most part, an increase in the hydrogen withdrawal rates with each cycle [13,20,23,24]; and [15]. These results from previous studies differ from what was observed in the base case of this study, where the hydrogen withdrawal rate decreased with increasing number of cycles, and in the water-bearing reservoir case where hydrogen withdrawal rate was constant for each cycle.

In the base case of this study, as the gas saturation increases, the mobility of both hydrogen and methane increases, allowing for increased withdrawal of methane because the model assumes the gases mix at reservoir conditions. The increase in methane withdrawal continues until water production becomes significant. Both hydrogen and methane withdrawal are affected by the increase in water production. In the case of hydrogen withdrawal from the water-bearing reservoir, although the hydrogen withdrawal rate is constant, the drawdown pressure increases, and water production increases with each cycle due to cresting effects.

There were, however, situations in our sensitivity analyses where we observed increasing hydrogen withdrawal rates with increasing cycle numbers. These occurred when the withdrawal well bottom hole pressure limit was reached (in all cases where the permeability was 10 mD, and when the reservoir was dipping at an angle of 10° with the well placed in the center of the reservoir rather than the well placed updip of the structure). Two of these scenarios are shown in Fig. 16. In these cases, hydrogen recovery was based on the volume of hydrogen available in the reservoir and not the reservoirs' ability to deliver the target withdrawal rate. Though the hydrogen withdrawal rate increased with increase in cycles in these cases, the amount of energy required to deliver the hydrogen is large (large drawdowns). Hence the scenarios are not considered optimal for hydrogen withdrawal. These findings imply that hydrogen withdrawal per cycle could either increase or decrease depending on the reservoir management practice, structure, or reservoir properties.

Proposed site selection criteria for hydrogen storage in depleted gas reservoirs

Based on the numerical simulation study findings and information available in the literature, we propose site selection criteria for hydrogen storage in depleted gas reservoirs. Developing the site selection criteria follows a similar approach taken by Ref. [41] for carbon dioxide storage. The high-level site selection criteria adapted for underground hydrogen storage involve three stages. In stage 1, fields are screened to determine if they qualify for underground hydrogen storage. Then in stage 2, relevant parameters are rated and ranked to identify top-performing sites. We assume the depleted gas reservoir is a sandstone reservoir. Table 6 summarizes parameters that can be used as screening criteria, while Table 7 shows our proposed ranking criteria when there exists more than one field to select from. In situations where sites may have similar parameters, and all (or most) may fall into a given score listed in Table 7, we suggest that users can add further granularity to the site scoring process based on the data they have. For instance, if five sites to be scored all have flow capacities between 1300 mD and 9000 mD, instead of giving all five sites a score of 2, the user can decide to create a new scoring criterion bearing in mind

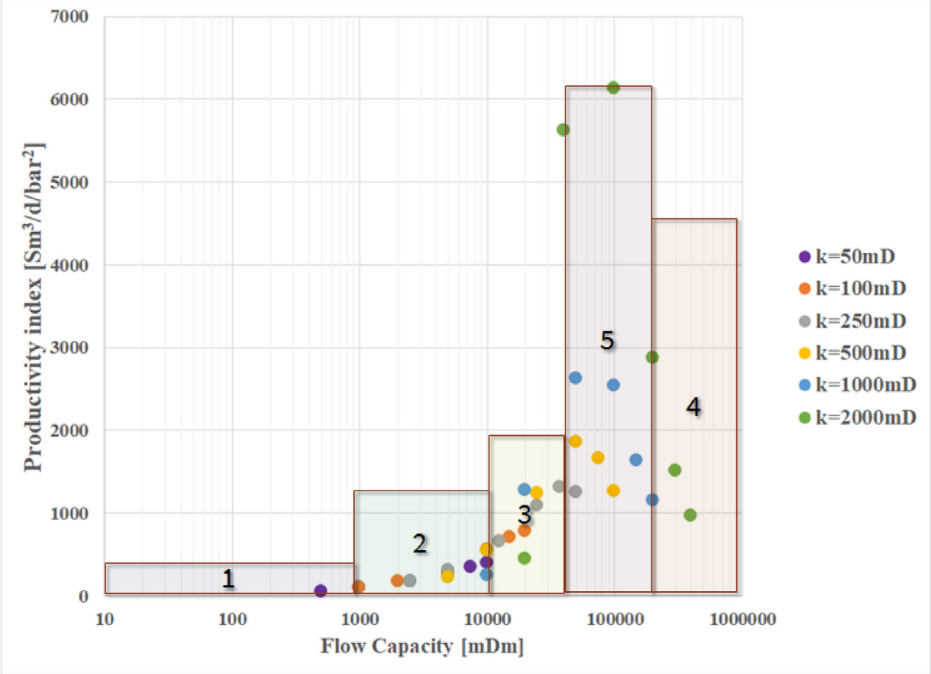

Fig. 17 – Hydrogen productivity index versus flow capacities for various formation permeabilities grouped by flow capacities to develop a rating criterion for underground hydrogen storage site selection.

that reservoirs with larger flow capacities may be more suitable for underground hydrogen storage than reservoirs will small flow capacities.

We determined the rating criterion for flow capacity by grouping the flow capacities based on ranges of PIs. Fig. 17 is a modified form of Fig. 10(d) and includes the ranges for the rating criterion.

Conclusion

In this study, we investigated the behavior of hydrogen injection, storage and withdrawal in a typical depleted gas reservoir. We used a reservoir simulator combined with sensitivity analyses to better understand the geological, reservoir, and operational controls that impact the productivity of hydrogen withdrawn. We also studied how the behavior differs if the storage formation was a saline reservoir.

We deduced that reservoirs with smaller current reservoir pressures (less than 50 bar) are more suitable for hydrogen storage if surface pressure constraints, such as well head pressure constraints, can be met. Shallow reservoirs (about 500 m) are also preferred for hydrogen storage if the reservoir pressure can support fluid flow and the reservoir has the capacity for the gas. Steeply dipping reservoirs enable better hydrogen recovery if the reservoirs have good permeability (greater than 100 mD) and the injection/withdrawal well is placed updip of the reservoir structure. Permeable reservoirs and reservoirs with sufficient thickness increase hydrogen withdrawal rates and the fraction of injected hydrogen withdrawn.

Subsequently, we combined the findings of this study with information in the literature to develop a set of site selection criteria for hydrogen storage in depleted reservoirs.

Overall, we have demonstrated that numerical simulation is valuable for understanding the dynamics associated with hydrogen storage in depleted reservoirs and is useful to determine the optimal conditions for maximizing hydrogen recovery from storage sites. Further research is needed to replicate the detailed sensitivity analyses using typical saline reservoir conditions to determine the selection criteria for potential saline reservoirs for hydrogen storage.

Declaration of competing interest

The authors declare that they have no known competing financial interests or personal relationships that could have appeared to influence the work reported in this paper.

Acknowledgments

The authors acknowledge Southern Company and the Stanford Center for Carbon Storage for funding; Jimin Daniel Zhou of Stanford University for providing the codes used to compute the binary interaction coefficients for this study; Mohammed Jabs Aljubran for fitting the hydrogen solubility equation to existing data; Michael Williams and Marie Ann Giddins of Schlumberger for providing guidance on how to use ECLIPSE E300 to model hydrogen storage and extraction, and Wolf Tilmann Pfeiffer, Firdovsi Gasanzade, and Sebastian Bauer of Kiel University for sharing sample numerical models for hydrogen storage for model validation.

Appendix A. Supplementary data

Supplementary data to this article can be found online at https://doi.org/10.1016/j.ijhydene.2022.07.239.

REFERENCES

[1] Panfilov M. 4 - underground and pipeline hydrogen storage. In: Energy WP, Gupta RB, Basile A, Veziroğlu NT, editors. Hydrogen storage, transportation and Infrastructure. Compendium of hydrogen energy, vol. 2. Woodhead Publishing; 2016. p. 91–115.
[2] Andersson J, Grönkvist S. Large-scale storage of hydrogen. Int J Hydrogen Energy 2019;44(Issue 23):11901–19.
[3] Langmi HW, Engelbrecht N, Modisha PM, Bessarabov D. Chapter 13 - hydrogen storage. In: Smolinka T, Garche J, editors. Electrochemical power sources: Fundamentals, systems, and Applications. Elsevier; 2022. p. 455–86.
[4] Zivar D, Kumar S, Foroozesh J. Underground hydrogen storage: a comprehensive review. Int J Hydrogen Energy 2021:23436–62.
[5] Foh S, Novlin M, Rockar E, Randolph P. Underground hydrogen storage. Chicago, USA: Institute of Gas Technology; 1979.
[6] Dopffel N, Jansen S, Gerritse J. Microbial side effects of underground hydrogen storage – knowledge gaps, risks and opportunities for successful implementation. Int J Hydrogen Energy 2021;46:8594–606.
[7] Heinemann N, Alcalde J, Miocic JM, Hangx S, Kallmeyer J, Ostertag-Henning C, al e. Enabling large-scale hydrogen storage in porous media-the scientific challenges. Energy Environ Sci 2021;14:853–64.
[8] Muhammed NS, Haq B, Al Shehri D, Al-Ahmed A, Rahman MM, Zaman E. A review on underground hydrogen storage: insight into geological sites, influencing factors and future outlook. Energy Rep 2022:461–99.
[9] Osman AI, Mehta N, Elgarahy AM, Hefny M, Al-Hinai A, Al-Muhtaseb AH, al e. Hydrogen production, storage, Utilisation and environmental impacts: a review. Springer International Publishing; 2021.
[10] Pan B, Yin X, Ju Y, Iglauer S. Underground hydrogen storage : influencing parameters and future outlook. Adv Colloid Interface Sci 2021;294.
[11] Thaysen EM, McMahon S, Strobel GJ, Butler IB, Heinemann N, al e. Estimating microbial growth and hydrogen consumption in hydrogen storage in porous media. Renew Sustain Energy Rev 2021;151.
[12] Pfeiffer WT, Bauer S. Subsurface porous media hydrogen storage - scenario development and simulation. Energy Proc 2015:565–72.
[13] Pfeiffer WT, al Hagrey SA, Köhn D, Rabbel W, Bauer S. Porous media hydrogen storage at a synthetic, heterogeneous field site: numerical simulation of storage operation and geophysical monitoring. Environ Earth Sci 2016;75(16):1177.
[14] Pfeiffer WT, Beyer C, Bauer S. Hydrogen storage in a heterogeneous sandstone formation: dimensioning and induced hydraulic effects. Petrol Geosci 2017:315–26.

[15] Lysyy M, Fernø M, Ersland G. Seasonal hydrogen storage in a depleted oil and gas field. Int J Hydrogen Energy 2021;46(49):25160–74.
[16] Wang G, Pickup G, Sorbie K, Mackay E. Scaling analysis of hydrogen flow with carbon dioxide cushion gas in subsurface heterogeneous porous media. Int J Hydrogen Energy 2022;47(3):1752–64.
[17] Kanaani M, Sedaee B, Asadian-Pakfar M. Role of cushion gas on underground hydrogen storage in depleted oil reservoirs. J Energy Storage 2022;45.
[18] Zamehrian M, Sedaee B. Underground hydrogen storage in a partially depleted gas condensate reservoir: influence of cushion gas. J Petrol Sci Eng 2022;212.
[19] Hagemann B, Rasoulzadeh M, Panfilov M, Ganzer L, Reitenbach V. Mathematical modeling of unstable transport in underground hydrogen storage. Environ Earth Sci 2015:6891–8.
[20] Feldmann F, Hagemann B, Ganzer L, Panfilov M. Numerical simulation of hydrodynamic and gas mixing processes in underground hydrogen storages. Environ Earth Sci 2016:1–15.
[21] Amid A, Mignard D, Wilkinson M. Seasonal storage of hydrogen in a depleted natural gas reservoir. Int J Hydrogen Energy 2016:5549–58.
[22] Hagemann B, Rasoulzadeh M, Panfilov M, Ganzer L, Reitenbach V. Hydrogenization of underground storage of natural gas: impact of hydrogen on the hydrodynamic and bio-chemical behavior. Comput Geosci 2016:595–606.
[23] Sainz-Garcia A, Abarca E, Rubi V, Grandia F. Assessment of feasible strategies for seasonal underground hydrogen storage in a saline aquifer. Int J Hydrogen Energy 2017:16657–66.
[24] Luboń K, Tarkowski R. Numerical simulation of hydrogen injection and withdrawal to and from a deep aquifer in NW Poland. Int J Hydrogen Energy 2020:2068–83.
[25] Mahdi DS, Al-Khdheeawi EA, Yuan Y, Zhang Y, Iglauer S. Hydrogen underground storage efficiency in a heterogeneous sandstone reservoir. Advances in Geo-Energy Research 2021:437–43.
[26] Scafidi J, Wilkinson M, Gilfillan SM, Heinemann N, Haszeldine SR. A quantitative assessment of the hydrogen storage capacity of the UK continental shelf. Int J Hydrogen Energy 2021;46(12):8629–39.
[27] Iglauer S. Optimum geological storage depths for structural H2 geo-storage. J Petrol Sci Eng 2022;211. https://doi.org/10.1016/j.petrol.2021.109498.
[28] Hassanpouryouzband A, Joonaki E, Edlmann K, Haszeldine RS. Offshore geological storage of hydrogen: is this our best option to achieve net-zero? ACS Energy Lett 2021:2181–6.
[29] Bouteldja M, Acosta T, Carlier B, Reveillere A, Jannel H, Fournier C. Definition of selection criteria for a hydrogen storage Site in depleted Fields or aquifers. 2021, March. Retrieved from hystories: https://hystories.eu/wp-content/uploads/2021/05/D1.1-0-Selection-criteria-for-H2-storage-sites.pdf.
[30] Jahanianfard D, Planning AP, Nemati B, Mapar M, Davarazar P, Zandi S, Mohammadi M. A sustainable approach for site selection of underground hydrogen storage facilities using fuzzy-delphi methodology. Mater Sci 2019.
[31] Newman GH. Pore-volume compressibility. J Petrol Technol 1973:129–34.
[32] Schlumberger. ECLIPSE technical Description. 2016. Version 2016.2.
[33] Qian J-W, Jaubert J-N, Privat R. Phase equilibria in hydrogen-containing binary systems modeled with the Peng–Robinson equation of state and temperature-dependent binary interaction parameters calculated through a group-contribution method. J Supercrit Fluids 2013;5:58–71.
[34] Lemmon EW, Bell IH, Huber ML, McLinden MO. In: Linstrom PJ, Mallard WG, editors. Thermophysical properties of Fluid systems. *NIST Chemistry WebBook, NIST standard Reference Database number 69*. of standards and technology. Gaithersburg, MD: National Institute; 2021. Retrieved, . [Accessed 2 September 2021].
[35] Yekta AE, Manceau JC, Gaboreau S, Pichavant M, Audigane P. Determination of hydrogen-water relative permeability and capillary pressure in sandstone: application to underground hydrogen injection in sedimentary formations. Transport in Porous Media; 2018. p. 333–56.
[36] Wiebe R, Gaddy VL. The solubility of hydrogen in water at 0, 50, 75 and 100° from 25 to 1000 atmospheres. J Am Chem Soc 1934;56(1):76–9.
[37] Culberson OL, McKetta JJ. Phase equilibria in hydrocarbon-water systems III - the solubility of methane in water at pressures to 10,000 PSIA. J Petrol Technol 1951;3:223–6.
[38] Kastor RL, Letbetter SC. Extra increments of pressure or mud Weight safety factors added during well Killing Procedures can Be Unsafe. *Paper presented at the*. In: *Fall* meeting of the society of Petroleum Engineers of AIME; 1974. Houston, Texas.
[39] AAPG. Fluid flow fundamentals. 2022, January 19. Retrieved from AAPG Wiki: https://wiki.aapg.org/Fluid_flow_fundamentals#cite_ref-pt10r7_3-0.
[40] Douglas JM. Conceptual design of chemical processes. New York: McGraw-Hill; 1988.
[41] Callas C. Development and application of site selection criteria for offshore carbon Sequestration. Stanford Center for Carbon Storage Annual Meeting; 2021, November.
[42] Kim TW, Callas C, Saltzer SD, Kovscek AR. Assessment of oil and gas fields in California as potential CO2 storage sites. Int J Greenh Gas Control 2022.